Proton Chelating Ligands Drive Improved Chemical Separations for Rhodium

Proton Chelating Ligands Drive Improved Chemical Separations for Rhodium

Hirokazu Narita,[a,*] Rebecca M. Nicolson,[b] Ryuhei Motokawa,[c] Fumiyuki Ito,[a] Kazuko Morisaku,[a] Midori Goto,[a] Mikiya Tanaka,[a] William T. Heller,[d] Hideaki Shiwaku,[c] Tsuyoshi Yaita,[c] Ross J. Gordon,[e] Jason B. Love,[b] Peter A. Tasker,[b] Emma R. Schofield,[e] Mark R. Antonio,[f] and Carole A. Morrison[b,*]

[a] Environmental Management Research Institute, National Institute of Advanced Industrial Science and Technology (AIST), 16-1 Onogawa, Tsukuba, Ibaraki 305-8569, Japan.

[b] EaStCHEM School of Chemistry, University of Edinburgh, The King's Buildings, David Brewster Road, Edinburgh EH9 3FJ, UK.

[c] Materials Sciences Research Center, Japan Atomic Energy Agency (JAEA), Tokai, Ibaraki 319-1195, Japan.

[d] Neutron Scattering Division, Oak Ridge National Laboratory, Oak Ridge, TN 37831, USA

[e] Johnson Matthey Technology Centre, Sonning Common, Reading, RG4 9NH, UK.

[f] Chemical Sciences and Engineering Division, Argonne National Laboratory, 9700 South Cass Avenue, Lemont, USA.

Corresponding author emails: c.morrison@ed.ac.uk, hirokazu-narita@aist.go.jp

Abstract

Current methods for the extraction of rhodium carry the highest carbon footprint and worst pollution metrics of all of the elements used in modern technological applications. Improving upon existing methods is made difficult by the limited understanding of the molecular-level chemistry occurring in these processes, particularly in the hydrometallurgical separation step. While many of the precious metals can be separated by solvent extraction, there currently exist no commercial extraction reagents for Rh. This is due to its complicated mixed speciation upon leaching into hydrochloric acid, which gives rise to difficulties in designing effective reagents for solvent extraction. Herein we show that the diamidoamine reagent N-n-hexyl-bis(N-methyl-N-n-octyl-ethylamide)amine transports Rh(III) from aqueous HCl into an organic phase as the mono-aquated dianion $[RhCl_5(H_2O)]^{2-}$ through the formation of an outer-sphere assembly; this assembly has been characterized by experimentation (slope analysis, FT-IR and NMR spectroscopy, EXAFS, SANS, ESI-MS) and computational modeling. The paper demonstrates the importance of applying a broad range of techniques to obtain

a convincing mode of action view for the complex processes involved in anion recognition in the solution phase. A consistent and comprehensive understanding of how the ligand operates to achieve Rh(III) selectivity over the competitor anion Cl^- has emerged. This knowledge will guide the rational design of the next generation of extractants and thus offers promise for improving the sustainability of metal extraction from both traditional mining sources and the recycling of secondary source materials.

Introduction

Metals are widespread in today's society, with their fundamental properties increasingly exploited to improve the performance and reliability of new technologies.[1] Forty years ago the number of elements present in a typical electronic device was around twelve; now it is greater than sixty, meaning that just about every element that is not radioactive, water-soluble or gaseous finds an application in materials science.[2]

Rhodium is a platinum group metal (PGM) which, along with platinum and palladium, primarily finds application in catalytic convertors in engine exhausts. Life cycle analysis for the production of PGMs has revealed that they carry a very high environmental burden, with rhodium production shouldering by far the highest global warming potential (due to fossil fuel energy consumption) and pollution metrics (measured in terms of terrestrial acidification, freshwater eutrophication and human toxicity) of all elements mined from virgin ores.[3] The high value of PGMs has created a market for their recovery from end-of-life products, with current recycling rates of these elements estimated to be above 50%.[4]

The production of metals such as rhodium involves ore mining or secondary resource recycling. Both usually require extensive refining, using methods such as smelting to concentrate the metal source, followed by hydrometallurgy to separate and obtain the metals in their elemental form. Hydrometallurgy dissolves, or leaches, the metal concentrate using aqueous acid, then employs a separation process such as solvent extraction[5] followed by reduction of the single metal streams.

For rhodium, the most effective leaching uses hydrochloric acid under oxidative conditions and, depending on the rhodium and chloride concentrations, temperature and pH, a mixture of chlorido- and aquochlorido-complexes, e.g. $[RhCl_n(H_2O)_{6-n}]^{3-n}$, can form.[6, 7, 8] This variety of species makes Rh separation using solvent extraction difficult as the tailoring of the organic-phase extractant becomes impractical. The chloridometalates are kinetically inert, so in order to gain separation extractants are designed to target the outer coordination sphere; the presence of multiple aquated chloridometalate species is therefore a significant complicating factor in extractant design. At present, there are no commercial extractants for the separation and recovery of rhodium. As such, in current processes, *e.g.* the Vale Process, all other PGMs are recovered from the stream first,[9] with rhodium then isolated by precipitation.[9b] Alternatively, the Rh chloride stream can be reduced by the addition of Sn(II) to generate more hydrophobic mixed-metal species, which are easier to recover by solvent extraction but subsequently require Sn/Rh separation.[6, 10]

The most effective way to generate charge-neutral assemblies of chloridometalates that are soluble in the water-immiscible phase in a solvent extraction process is to form ion pairs with cationic forms of

the extractant.[5] This results in an equilibrium for the loading and stripping stages that is pH-dependent (Equation 1). In practice, this equilibrium operates only when $n > 3$ because only metalate anions can be extracted by the protonated reagent to give charge neutral, hydrocarbon-soluble species. Introducing amido groups into the extracting reagents has been demonstrated to favour transport of MCl_x^{y-} over Cl^-, which is always present in large excess in streams resulting from oxidative chloride leaching.[11] In many cases this selectivity of transport appears to be a consequence of the added proton being chelated by the amide oxygen atom, reducing its availability to interact with the charge dense (hard) chloride ion. The proton chelation often templates the cation to provide an array of polarised $N\text{-}H^{\delta+}$ and $C\text{-}H^{\delta+}$ units to interact with centres of negative charge on the charge diffuse (soft) chloridometalate anions.[11a]

$$[RhCl_n(H_2O)_{6-n}]^{(n-3)-} + (n-3)L_{(org)} + (n-3)H^+ \rightleftharpoons [RhCl_n(H_2O)_{6-n}]\cdot(LH)_{n-3(org)} \qquad \text{Equation 1}$$

Most studies to date that address the mode of action of extraction of chloridometalate anions have involved symmetrical anions such as $AuCl_4^-$, $ZnCl_4^{2-}$ and $PtCl_6^{2-}$,[11] in which the whole of the outer coordination sphere is composed of identical hydrogen-bond acceptor groups. One of the features of interest in the extraction of Rh(III) considered in this paper is that the mono-aquo complex $[RhCl_5(H_2O)]^{2-}$, or other metalates e.g. $[RhCl_4(H_2O)(OH)]^{2-}$ or $[RhCl_4(H_2O)_2]^-$, could function as a ditopic guest in which the bound water molecule(s) provide a hydrogen-bond donor site and the chloride ions function as acceptor sites. There is precedent for this in the formation of an amide-Er(III) complex in which an amide oxygen atom interacts in the outer sphere with a coordinated water molecule.[12] Previous work has also shown that the mono-, di- and triamido-substituted tertiary amines (**L1-3**, Figure 1) recover Rh from aqueous HCl by solvent extraction and that they are stronger extractants for Rh than trioctylamine (**toa**), which is a model for the commercial Alamine® reagent.[13] The strength has been shown to vary in the order triamide (**L3**) ≥ diamide (**L2**) >> monoamide (**L1**). The amidoamines **L1-3** are rare examples of reagents capable of selectively recovering Rh from aqueous HCl, and could conceivably be introduced into a solvent extraction flowsheet for the PGMs to ensure efficient recovery of each PGM. However, revealing the intricacies of complex fluid systems, such as those operating in the selective transport of Rh chloridometalates from an acidic aqueous phase to a immiscible hydrophobic phase, requires a comprehensive joint experimental and computational modelling investigation.[14] This complete chemical and atomistic analysis of selective metalate transport should provide fundamental understanding that can be exploited in the future design of chemical extractants and their integration into complete metal recovery circuits.

In this paper a broad range of analytical, spectroscopic, and computational modelling techniques are brought together to investigate the mode of action of **L2** and to explain why it is a stronger extractant than a simple amine (**toa**) and the monoamide (**L1**), and similar in strength to the triamide (**L3)**. Extractant behavior in both chloroform and 1-octanol are explored and found to give consistent results, with both suppressing formation of a third phase or formation of precipitates. The phenyl-substituted analogue (**L4**) of the diamide (**L2**) has also been used to prepare crystalline complexes for X-ray structure determination.

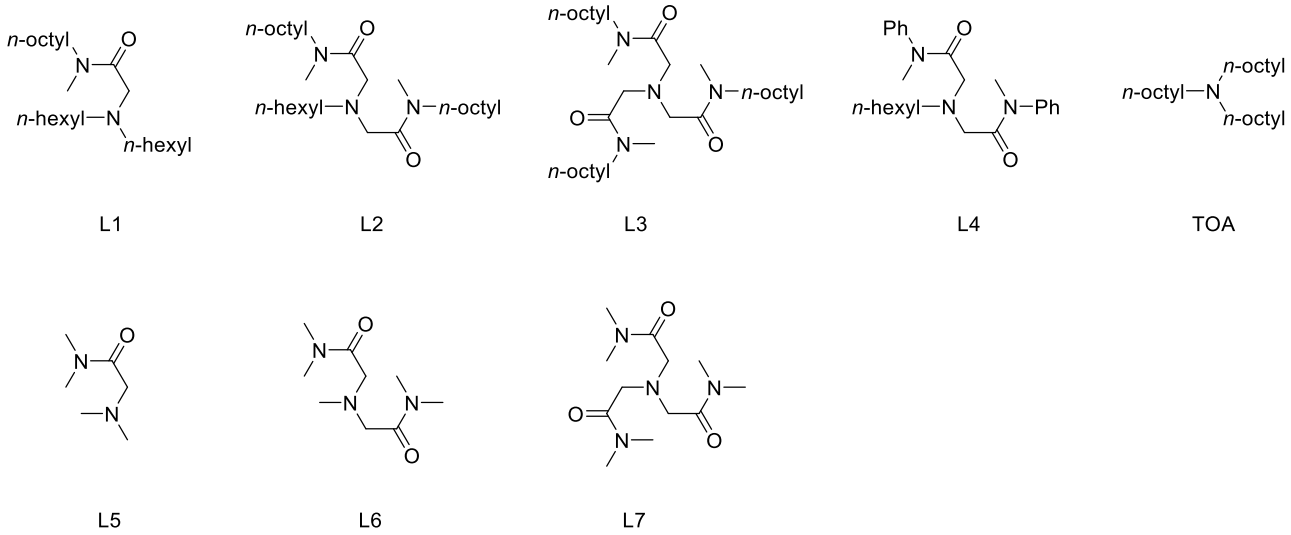

Figure 1. Structures of *N*,*N*-di-*n*-hexyl(*N*-methyl-*N*-*n*-octyl-ethylamide)amine (**L1**), *N*-*n*-hexyl-bis(*N*-methyl-*N*-*n*-octyl-ethylamide)amine (**L2**), tris(*N*-methyl-*N*-*n*-octyl-ethylamide)amine (**L3**), *N*-*n*-hexyl-bis(*N*-methyl-*N*-phenyl-ethylamide)amine (**L4**) and **toa**, along with the truncated forms (R-groups reduced to methyl groups) for computational work (**L5**, **L6** and **L7**).

Experimental section

Reagents. A summary of the reagents employed, along with synthesis details for **L2** and **L4** can be found in the Supporting Information.

Solvent extraction (AIST data). The extractant solution was prepared by dissolving **L2** or **toa** in 1-octanol and contacted with 2.0 M HCl solution as follows: 2.0 mL of the organic solution along with 2.0 mL of 2.0 M HCl solution were placed in a 10 mL stopped glass tube and shaken vertically for 30 min using a mechanical shaker (amplitude = 100 mm, frequency = 200 strokes/min), and then

centrifuged. After this pre-equilibration step, H^+ concentration in the organic phase was calculated based on mass balance of the H^+ in the aqueous phase before and after shaking, which was determined by NaOH titration using an automatic potentiometric titrator (Kyoto Electronics AT-610). H^+ concentration in the organic phase was found to be near identical (≤ 0.02 M) for both **L2** and **toa**, for all concentrations of **L2** and **toa** (0.05-0.5 M) using 2.0 M HCl for the initial aqueous phase, implying that a 1:1 (**L2** or **toa**)/HCl complex was dominantly formed, concordant with the results obtained using chloroform as a diluent.[7] Rh(III) extraction was then carried out using 1.0 mL of the pre-equilibrated organic solution and 1.0 mL of a 2.0 M HCl solution containing Rh(III). The operation of Rh(III) extraction was the same as that for the pre-equilibration, except the shaking time was increased to 60 min, which was long enough to reach the extraction equilibrium. The concentration of Rh(III) was measured by ICP-AES (Horiba ULTIMA2), with values in the organic phase determined based on mass balance of the Rh(III) in the aqueous phase before and after extraction. The estimated uncertainty in the concentrations of the Rh(III) samples was <5%. All extraction experiments were done at 23±1˚C and performed in triplicate. The distribution ratio (*D*) was calculated from Equation 2, where $[M]_{init,aq}$, $[M]_{eq,org}$, and $[M]_{eq,aq}$ denote the metal concentration in the initial aqueous phase, the equilibrated organic phase after extraction and the equilibrated aqueous phase after extraction, respectively.

$$D = [M]_{eq,org}/[M]_{eq,aq} = ([M]_{init,aq} - [M]_{eq,aq})/[M]_{eq,aq} \quad \text{Equation 2}$$

Solvent extraction (University of Edinburgh data). The extractant solutions were prepared by dissolving **L2** in chloroform or deuterated-chloroform and stirring with equal volumes of 2.0 M aqueous HCl in small vials for 30 min and then centrifuged. After this pre-equilibration step, Rh(III) extraction was carried out using equal volumes of the pre-equilibrated chloroform solution and a 2.0 M aqueous HCl solution containing different concentrations of Na_3RhCl_6 under the same conditions as used for the pre-equilibration. NMR spectra were recorded on $CDCl_3$ solutions after five contacts with 2.0 M HCl solution containing Rh(III) solution to maximize the Rh(III) concentration in the organic phase. The concentration of Rh(III) in the organic phase was measured directly by ICP-OES (Perkin Elmer Optima 5300DC).

FT-IR spectroscopy: All FT-IR spectra were collected using a PerkinElmer Spectrum 100 instrument. Liquid samples based on the **L2** ligand system were prepared in organic media (see Supporting Information), as well as neat, and placed in a System Engineering diamond compression cell for data collection. All the solution samples were measured within 3 days after the preparation. Pellets of crystalline **L4** and [$RhCl_3$(**L4**)] were also prepared for analysis by grinding with KBr.

X-ray Diffraction: Crystals of **L4** were prepared by dissolving (1 g) in 10 ml of methanol and allowing the solution to stand for 1 day at room temperature. For **L4**-Rh, crystals were prepared as follows: **L4** (1.58 g, 0.0040 mol) was dissolved in 20 mL of methanol. To this solution was added a solution of $RhCl_3 \cdot 3H_2O$ (0.53 g, 0.0020 mol) in 60 mL of methanol. The mixture was stirred at room temperature for 16 h, and the solvent was removed *in vacuo*. The residue was suspended in ethylacetate/hexane (2/3) and the solid material dissolved in chloroform. The solution was washed with water and dried over anhydrous sodium sulfate. After the solvent had been removed in vacuo, the resulting semi crystalline material was dissolved in chloroform/methanol (10/1) and the solution was left to stand for 120 h at 5 ˚C to give orange crystals that were suitable for single crystal X-ray diffraction studies. A suitable crystal of **L4** was mounted on a glass fiber, and that for the **L4**-Rh complex was sealed in a glass capillary. The measurements were carried out at 183 K on a Bruker SMART AXS CCD 5.625 diffractometer equipped with graphite monochromated Mo-Kα radiation (λ = 0.71073 Å). The structures were solved by direct methods and refined on F^2 by full-matrix least-squares techniques using SHELXL-2014.[15] All non-hydrogen atoms were refined anisotropically. All the hydrogen atom positions were calculated. CrystalMaker for Windows version 2.2.0 was employed for molecular graphics.[16] Crystallographic data are provided in the Supporting Information.

Extended X-ray Absorption fine structure (EXAFS): Two independent sets of EXAFS measurements were performed in this work. For set 1, a single aqueous sample of 0.1 M Rh(III) in 2 M HCl was measured, alongside organic (1-octanol) samples obtained from 0.5 M **L2** contacted with 0.1 M Rh(III) in 2 HCl ($[Rh]_{eq.org}$ = 0.06 M) and 1.0 M **toa** contacted with 0.1 M Rh(III) in 2 M HCl ($[Rh]_{eq.org}$ = 0.06 M) 3-4 days after preparation. A further sample of Rh(III)**L2**, obtained as an oil following a prolonged reaction between $RhCl_3 \cdot 3H_2O$ and **L2** in methanol, was also analysed (see Supporting Information). Crystalline samples of the Rh-**L4** complex were also prepared for EXAFS analysis by grinding with boron nitrate and pelleted. For set 2, a series of ca. 0.01 M Rh(III) aqueous samples were prepared from Na_3RhCl_6 under varying HCl conditions (2, 4 and 10 M HCl). To this list were added two organic (d-chloroform) samples containing 0.1 M **L2**, analyzed either 1 or 6 months after multiple contacts with a 2 M HCl phase containing 0.1 M Rh(III).

Data collection (Set 1): Rh K-edge EXAFS spectra were collected in transmission mode at BL11XU equipped with a Si(111) crystal monochromator of the SPring-8 (8 GeV at ~99 mA). Monochromator energy calibration was carried out using Rh metal foil (23220 eV). All the measurements were performed at 25 ˚C. All solutions were transferred to 2-10 mm diameter polyethylene cells, which were then tightly sealed. Both ion chambers (placed before and after the sample in the beam path)

were filled with N_2. The beam size on the sample was about 1 × 1 mm^2. 2–5 five-minute scans in QEXAFS mode to k_{max} = 18 $Å^{-1}$ were averaged for each sample. Details regarding the data processing procedure can be found in the Supporting Information.

Data collection (Set 2): Rh K-edge X-ray absorption spectra were collected in fluorescence mode at beamline B18, the Core-XAS beamline at the Diamond Light Source, using a Canberra 36-element Germanium detector with XSPRESS2 readout electronics. Data were acquired using a double crystal monochromator with Si(311) crystals, and Pt coated mirrors for beam collimation and focusing. The beam size on the sample was adjusted to have a footprint of approximately 1 × 1 mm^2. The incident X-ray energy was calibrated against the first inflection point of the K-edge of Rh foil. All solutions were contained in glass capillary tubes, 3 mm diameter for measurements in a gas exchange liquid nitrogen cryostat at 90 K. 10 to 40 three-minute scans in QEXAFS mode to k_{max} = 15 $Å^{-1}$ were averaged for each of the solutions. Details regarding the data processing procedure can be found in the Supporting Information.

NMR spectroscopy: ^{1}H NMR spectra to confirm ligand synthesis were recorded at 300 K on a Bruker AVA500 spectrometer at 500.12 MHz. Spectra were referenced internally to residual protio solvent, and chemical shifts are reported in δ (ppm). 0.1 M **L2** (in chloroform and pre–contacted with 2 HCl) was contacted five times with 0.1 M Rh in 2 M HCl solution (equal volumes of each phase, stirring of 30 mins for each contact followed by centrifuging for 10 mins). Samples of the 0.1 M **L2** solution, the chloride loaded **L2** (from the pre-contact) and Rh loaded organic phases were analysed by ^{1}H NMR, ^{13}C NMR and ^{15}N NMR spectroscopy. The samples were approximately four months old at the time of analysis. ^{1}H, ^{1}H-^{1}H COSY, ^{13}C, ^{1}H-^{13}C HMBC, and ^{1}H-^{15}N HMBC spectra were recorded at 298 K on a Bruker AVA800 at 799.72 MHz. ^{1}H spectra were referenced internally to residual protio solvent, and chemical shifts are reported in δ (ppm).

Water content analysis. Karl Fischer titrations were employed to determine the water content of the equilibrium organic phases (1-octanol) after HCl/Rh(III) extraction. Densities of the measurement samples were checked using an Anton Paar DMA 35 densitometer and found to increase with increasing Rh(III) concentration: 0.88 g/mL for $[Rh]_{eq.org}$ = 0 M to 0.92 g/mL for $[Rh]_{eq.org}$ = 0.25 M for **L2**; 0.86 g/mL for $[Rh]_{eq.org}$ = 0 M to 0.89 g/mL for $[Rh]_{eq.org}$ = 0.26 M for **toa**. An azeotropic distillation method was adopted utilizing a volumetric Karl Fischer titrator AQ-2200A equipped with moisture vaporizing device EV-200L (Hiranuma Sangyo Co., Ltd.). Aqualite RS-A (Hiranuma Sangyo Co., Ltd.) and dehydrated toluene were used as the Karl Fischer reagent and solvent for

vaporization, respectively. The water concentration of each sample was measured a minimum of five times. The organic solutions (**L2**/**toa** in 1-octanol) were found to be slightly hygroscopic even in the absence of HCl (1.9 M and 1.8 M of water extracted for 0.50 M of **L2** and 1.0 M of **toa**, respectively), whereas both neat extractants extract hardly any water (<0.1 M) into the organic phase. Hence, water contents of 1.9 M for **L2** and 1.8 M for **toa** in 1-octanol were regarded as equilibrium background values.

Small angle neutron scattering (SANS) measurements. SANS measurements were performed with the time-of-flight extended *q*-range SANS (EQ-SANS) spectrometer of the Spallation Neutron Source, Oak Ridge National Laboratory, USA.[17] Sample-to-detector distances of 4.0 m and 1.3 m were employed with a single band of neutrons with wavelengths, λ, 1.00-4.64 Å and 1.00-5.28 Å, respectively, which provide a momentum transfer, q (= $(4\pi/\lambda)\sin(\theta/2)$, where θ is the scattering angle), ranging from 0.01 $Å^{-1}$ to 3 $Å^{-1}$. The divergence of the incident beam was defined using a 25 mm diameter source aperture and a 10 mm diameter sample aperture in both configurations. The scattered neutrons were detected with a two-dimensional position-sensitive ^{3}He detector of 1.0 × 1.0 m, composed of tube detectors providing 256 × 192 pixels. Data reduction followed standard procedures, as implemented in the Mantid software package.[18] The scattering data were corrected for wavelength-dependent sample transmission, for detector counting efficiency, and for instrumental background on a pixel-to-pixel basis. The reduced scattered intensity was then azimuthally averaged. Data output by the reduction were in absolute units of reciprocal centimeters through a scale factor determined by measuring a porous SiO_2 standard.[19] After subtracting the scattering contribution of the empty quartz cell from that of the sample, incoherent scattering from hydrogen, which was estimated as a constant value from the incoherent scattering intensity of a 2 mm thick H_2O reference sample in a quartz cell, was subtracted from the net absolute intensity.[20] The corrected scattered intensity distribution is designated as $I(q)$ hereafter. Here, note that $I(q)$ from 0.01 $Å^{-1}$ to 0.5 $Å^{-1}$ are used for quantitative data analysis due to a statistical error of the scattering intensity at q > 0.5 $Å^{-1}$. Details of sample preparations for SANS measurements are listed in the Supporting Information. Deuterated octanol, DCl and D_2O were used in the preparation of all samples to ensure sufficient neutron scattering contrast between solutes and diluent and to minimize the incoherent scattering background from hydrogen. Aliquots of all sample solutions were loaded into quartz cells of 2 mm sample thickness. All SANS data were acquired at 20°C.

ESI-Mass Spectrometry: Mass spectrometry measurements were undertaken to identify species formed in the organic (chloroform) phase for **L2** extractions from 0.1 M, 0.01 M and 0.001 M Rh(III) solutions (with lower Rh concentration solutions prepared from 0.1 M Na_2RhCl_6 in 2 M HCl stock

solution). 0.5 M **L2** in chloroform was prepared and pre–contacted with 2 M HCl. The organic phases were prepared by contacting the **L2** solution with the three aqueous solutions (equal volume contacts for 30 minutes, followed by 10 mins of centrifuging). These samples were analysed within 48 hours. Analysis of the organic phase from the extraction from 0.1 M Rh in 2 M HCl solution was repeated after seven months. In addition, a short contact organic phase was prepared by contacting 0.1 M Na_2RhCl_6 in 2 M HCl solution with 0.1 M **L2** in chloroform solution (30 second manual shake, no centrifuging to minimise contact time, total contact time of about a minute). This sample was analysed immediately. Mass spectrometry was carried out on a Thermo-Fisher LCQ Classic spectrometer (ESI). Organic phase samples were prepared for analysis by dilution in acetonitrile.

Computational modelling: Geometry optimization and frequency calculations were carried out using the Gaussian 09 program (versions EM64L–G09RevA.02 and EM64L–G09RevE.01).[21] The M06[22] exchange/correlation functional was used throughout, coupled to the LANL2TZ basis set and corresponding pseudo potential for Rh and the 6-311+G(d,p) basis set for all other elements. Polarisation continuum models (SCRF(solvent = water or chloroform), as appropriate) were used to model the solvation of the molecules and assemblies. Octyl and hexyl R-groups for **L1**-**L3** were replaced with methyl groups throughout to reduce computational expense and to aid structure optimisation, as the presence of long chain side groups considerably increases the probability of many similar energy local minima. Optimisation was carried out from a variety of starting structures, which were built based on the conformations of the extractants and on the possible binding modes that could occur to an anion (see Supporting Information). Different conformations of LH^+ were used and placed in different orientations around chloride or $[RhCl_5(H_2O)]^{2-}$. Structures were considered optimized when the forces and atomic displacements fell to within the program default convergence criteria or the opt = tight convergence criteria, with the exceptions of the **L**7H^+ and $[RhCl_5(H_2O)]\cdot$(**L7**(Me)H)$_2$ structures which failed to reach these criteria. For these two structures the structures corresponding to the lowest energies that could be obtained were carried forward for frequency calculations. Vibrational frequency calculations were carried out to verify that the optimum geometries found were minima and to obtain Gibbs free energy corrections. All structures were found to be minima with the exceptions of **L**7H^+ and $[RhCl_5(H_2O)]\cdot$(**L**7H)$_2$ (imaginary frequencies of 93.3594 cm^{-1}, and of 19.1911, 33.9988 and 49.7791 cm^{-1} and 30.6553 and 50.1588 cm^{-1}, respectively; imaginary eigenvectors suggested the source of the geometry optimisation problem stemmed from a competitive attraction for the amine H^+ by the three amide groups). Counterpoise correction calculations were carried out on the optimised geometries of the lowest energy structures for the **L**H·Cl and $[RhCl_5(H_2O)]\cdot$(**L**H)$_2$ assemblies and the energy correction was applied to energies used in the

calculation of formation or exchange energies.[23] See Supporting Information for details of the fragments defined in the counterpoise calculations. Ligand protonation energies, assembly formation energies and exchange energies were calculated using the difference in free energy values of the sum of the products and the sum of the individual reactants.

Results and discussion

Extraction of Rh(III): The dependence of the distribution ratios (*D*) of Rh(III) between 1-octanol and 2.0 M HCl on the concentrations of **L2** or **toa** (Figure 2) demonstrate that lower concentrations of **L2** than **toa** are required to achieve comparable Rh-loadings. The slopes of the log*D* *vs* log[*L*] plots (1.9 for **L2** and 2.1 for **toa**) indicate that 1:2 Rh(III):ligand complexes, consistent with $[RhCl_5(H_2O)]\cdot(LH)_2$, are the predominant species formed in the organic phase. The stoichiometry and the relative extraction efficiency (**L2** > **toa**) are the same as those observed in chloroform.[6] Extraction involving a 1:2 stoichiometry of Rh:**L2** could in theory result from transport of other dianionic species, but in the chloridoaquo-rhodium system the only reasonable possibility would be the ternary complex, $[RhCl_4(H_2O)(OH)]^{2-}$; this is only thought to exist at pH > 2.9,[24] not in the 2.0 M HCl solutions used here.

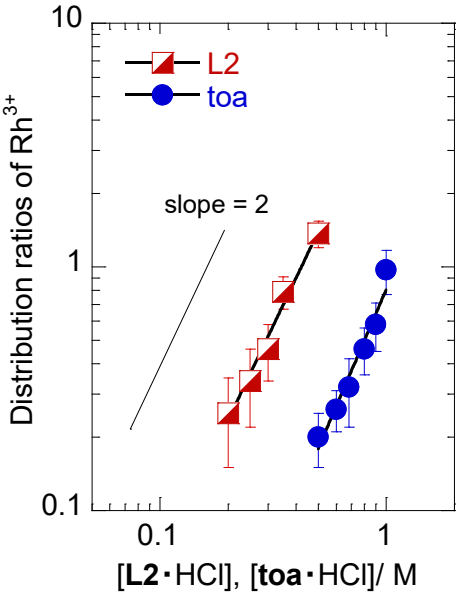

Figure 2. The dependence of the distribution ratio of Rh(III) on the concentrations of **L2** or **toa** (pre-equilibrated with 2.0 M HCl) in 1-octanol after contacting with an aqueous solution of $RhCl_3\cdot 3H_2O$ (10^{-3} M in 2.0 M HCl). Error bars represent 1σ.

FT-IR spectra and X-ray diffraction: The carbonyl stretching frequency ($\nu_{C=O}$) of the amide group in the diamides **L2** and **L4** was used to probe whether the oxygen atom entered the inner coordination

sphere of the rhodium atom on the timescales used for the extraction experiments. The spectra in Figure 3(a-e) indicate that when **L2** is dissolved in 1-octanol and is contacted with water, HCl, and subsequently used to extract rhodium, only minor shifts in frequency are observed compared to that for neat **L2** (1649 cm^{-1}). Whilst the shifts are small, they do reveal significant information. A slightly lower wave number shift from **L2** neat (a) was observed in **L2** in 1-octanol (b) and **L2** equilibrated with water (c), while the latter appear at similar wave number. This means that **L2** molecules interact with other **L2** molecules or 1-octanol, but no direct interaction occurs between water and the amide oxygen atoms in 1-octanol. The peak position and shape for **L2** after contact with HCl (d) is almost the same as for **L2** after contact with Rh(III) in HCl (e), implying that the coordination environment of the amide oxygen atoms does not change upon contact with Rh(III) and transport into the organic phase. This is consistent with the DFT calculations discussed below.

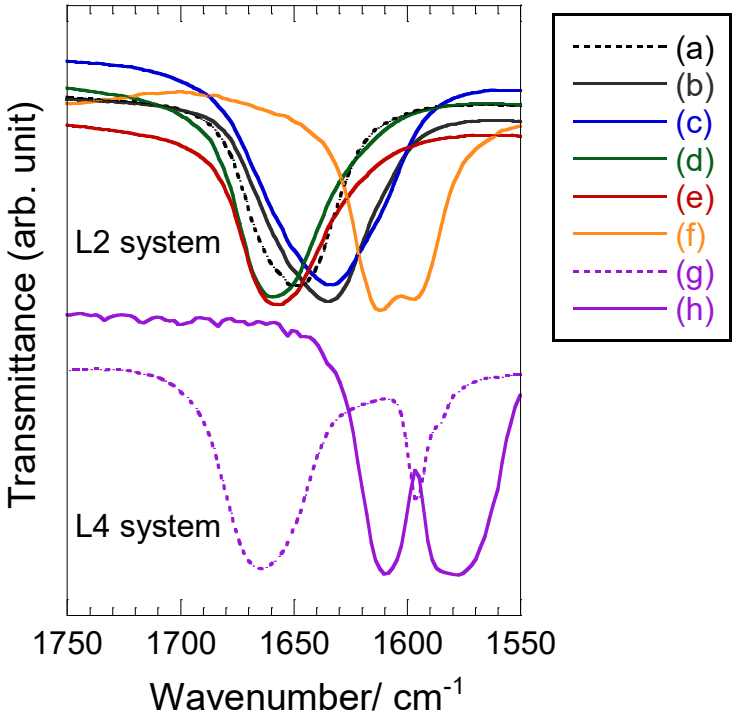

Figure 3. Amide carbonyl stretching frequencies for **L2** neat (a), a solution in 1-octanol (b) and solutions in 1-octanol after contacting with water (c), aqueous HCl (d) and aqueous $RhCl_3$/HCl (e) compared with the Rh-**L2** oily complex (no diluent) (f) and for **L4** (g) and *fac*-[$RhCl_3$(**L4**)] (h), as solids.

In contrast, a markedly different spectrum was obtained for (f), where a sample of the Rh complex was obtained as an oil following a prolonged reaction between $RhCl_3 \cdot 3H_2O$ and **L2** in methanol. In this spectrum the carbonyl stretching band is split and is similar to that (h) of the Rh complex bound to the model ligand **L4** (for which the uncoordinated spectrum is shown as (g)) obtained in a similar

manner. An X-ray structure of the latter (Figure 4 and Supporting Information) shows this to be *fac*-[$RhCl_3$(**L4**)] in which three inner coordination sphere sites are defined by the amine N-atom and two carbonyl O-atoms. A comparison with other related [$RhCl_3$(L)] complexes is presented in the Supporting Information.

Whilst the FT-IR spectra of extracts indicate that, in common with the extraction of most other PGMs as their chloridometalates, an outer sphere mechanism is involved initially, it is also possible that displacement of coordinated chloride ions can take place over time in the loaded organic phase. This needs to be recognized when using other techniques to probe the mechanisms of extraction and the structures of species formed.

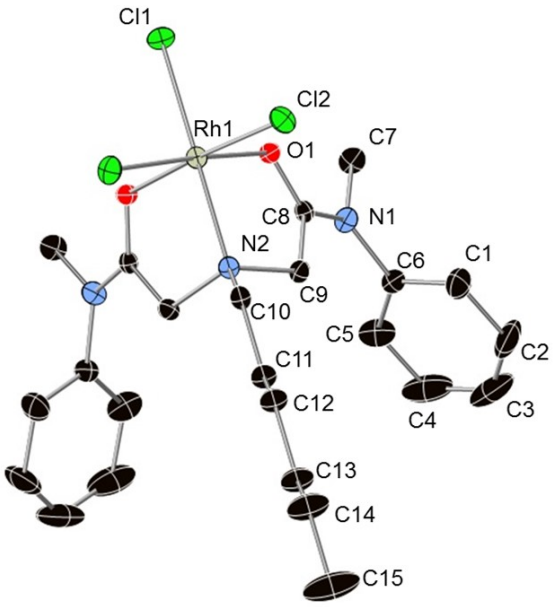

Figure 4. Part of the X-ray crystal structure of *fac*-[$RhCl_3$(**L4**)]. Ellipsoids are represented at the 30% probability level. H-atoms and those of $CHCl_3$ solvate molecules are omitted for clarity.

EXAFS: EXAFS data support the proposition that an outer sphere complex is first formed in Rh-extractions from 2 M aqueous HCl solutions. The spectra (b) and (c) in Figure 5 indicate that the coordination spheres of the rhodium atoms are very similar after extraction into 1-octanol by both **L2** and **toa.** They are also almost identical to that of the predominant Rh species in 2M aqueous HCl [spectra (a)].

Curve fitting to spectra (a), (b) and (c) in Figure 5 produces best–fit metrics that correspond to a 5:1 ratio of Cl : N/O atoms in the Rh coordination sphere (see Table 1 for summary, full table presented

in the Supporting Information). Spectra (d) and (e) take a very different form, having more prominent peaks arising from the lighter N/O atoms at shorter distances than those of the Rh-Cl bonds. This is indicative of inner-sphere binding in the [$RhCl_3$(**L4**)] complex and in the [$RhCl_3$(**L2**)] complex formed over a long time period, which is in accordance with the FT-IR measurements.

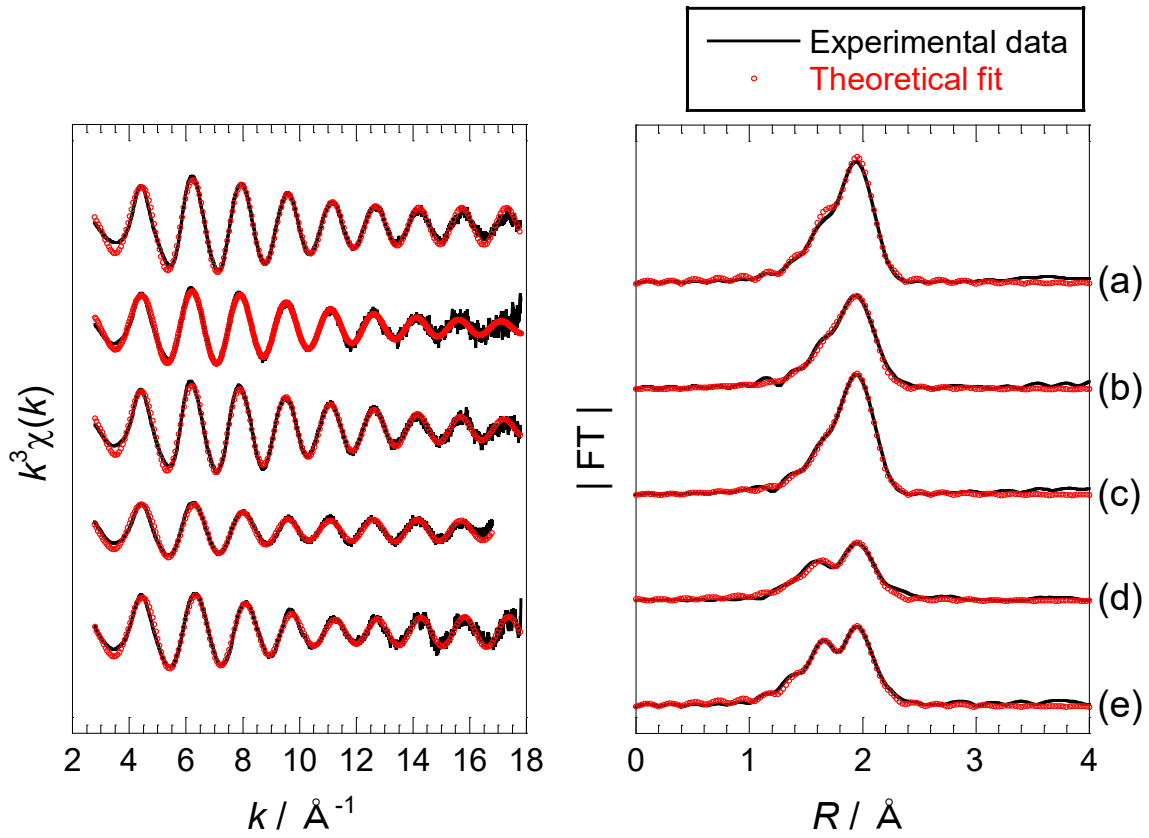

Figure 5. Rh K-edge k^3-weighted EXAFS (transmission mode) spectra and their Fourier transforms (phase shifts are not corrected) for (a) 0.1 M solution of $RhCl_3$ in aqueous HCl (2 M), (b) and (c) 1-octanol solutions of **L2**HCl (0.5 M) and **toa**H·Cl (1.0 M), respectively, after contact with an aqueous phase as in (a), (d) Rh-**L2** oily complex (no diluent) and (e) solid [$RhCl_3$(**L4**)].

The extraction data obtained thus far have assumed that the dominant speciation of Rh(III) in HCl is $[RhCl_5(H_2O)]^{2-}$. Validating this assertion is important because it can be assumed that the kinetic inertness of Rh(III) is such that there is insufficient time for interconversion of chloridoaquo complexes to take place in extractions carried out at room temperature with short contact times. To this end Rh K-edge EXAFS data were also collected for a series of solutions derived from Na_3RhCl_6 in varying HCl concentration. Plots of the Fourier transformations of the EXAFS data obtained for aqueous solutions with low Rh and varying HCl concentrations [samples (f)-(h), Table 1 and

Supporting Information], are dominated by one large peak at just under 2 Å; fitting shows this is consistent with a Rh-Cl distance of approximately 2.3 Å (phase corrected). At the lower HCl concentrations (samples (f) and (g), Table 1), the number of Cl atoms bound to Rh suggests that the solutions most likely contain a mixture of $[RhCl_6]^{3-}$ and $[RhCl_5(H_2O)]^{2-}$, with possibly much smaller quantities of $[RhCl_4(H_2O)_2]$ and $[RhCl_3(H_2O)_3]$. Whilst it is not possible to determine the proportion of each if there are more than two complexes present, the higher Cl number (6.1±0.6) for sample (h) suggests it consists of exclusively $[RhCl_6]^{3-}$, as might be expected for a 10 M HCl solution. If, as suggested by others,[6, 25] that aqueous HCl samples will contain a mixture of only $[RhCl_6]^{3-}$ and $[RhCl_5(H_2O)]^{2-}$, sample (f) will likely contain 50% of each, while sample (g) has 80% $[RhCl_6]^{3-}$ and 20% $[RhCl_5(H_2O)]^{2-}$. The presence of significant concentrations of $[RhCl_6]^{3-}$ is in line with ^{103}Rh NMR and HPLC-ICP-MS measurements[25-26] but is contrary to studies using UV/Vis spectroscopy and DFT calculations[6-7] Some of these disparities may have resulted from different Rh sources ($RhCl_3$ *versus* Na_3RhCl_6), or differences in concentration and sample preparation. Thus, whilst these results find agreement with the earlier studies that Rh(III) speciation in HCl media is complex, under the extraction operating conditions for **L2** explored in this paper it is likely that 50% of the Rh(III) present will be in the form of the dianion, and thus be extracted in a 1:2 ratio with **L2**, in agreement with the slope analysis presented in Figure 2.

Table 1. Summary of curve fitting for Rh-EXAFS data, where atom denotes the identity of the *N* atoms used in the fit and *R* the corresponding bond distance. The estimated standard deviations are reported (in parentheses) at the 2σ level for set 1 and 3σ-level for set 2.

Sample	[Rh] / M	[HCl] / M	Atom	*CN*	*R* / Å
Set 1					
(a). $RhCl_3$(aq)	0.1	2	O Cl	1.0(1)* 5.0(1)*	2.06(1) 2.328(4)
(b). 0.5 M **L2**H·Cl in octanol, after contact with solution (a).	0.06	-	O Cl	0.6(3) 5.3(6)	2.06(2) 2.342(9)
(c). 0.5 M **toa**H·Cl in octanol, after contact with solution (a)	0.06	-	O Cl	1.5(6) 3.8(6)	2.12(3) 2.352(6)
(d). Rh**L2** (oil)			O Cl	3.0(10) 3.0(10)	2.06(2) 2.34(2)
(e). $[RhCl_3$(**L4**)] (solid)	-	-	N/O	3#	2.06(1)

			Cl	3[#]	2.320(6)
Set 2					
(f). Na_3RhCl_6(aq)	0.006	2	Cl	5.5(7)	2.336(7)
(g). Na_3RhCl_6(aq)	0.007	4	Cl	5.8(5)	2.344(4)
(h). Na_3RhCl_6(aq)	0.007	10	Cl	6.1(6)	2.351(4)
(i). 0.1 M **L2**H·Cl in $CDCl_3$ after contact with 0.1 M Rh in 2 M HCl (sample aged by 1 month)	0.041	-	Cl Rh	5.4(5) 1.0(2)	2.347(4) 3.11(1)
(j). 0.1 M **L2**H·Cl in $CDCl_3$ after contact with 0.1 M Rh in 2 M HCl (sample aged by 6 months)	0.05	-	Cl Rh	5.3(7) 0.9(3)	2.348(6) 3.11(2)

[*] Set to equal 6.

[#] Fixed parameter.

An interesting feature was observed when EXAFS measurements were carried out on chloroform solutions of **L2** loaded from an aqueous solution containing a higher (0.1 M) concentration of rhodium than present in the aqueous samples (f)-(h) listed in Table 1. In these cases [samples (i) and (j)] the large peak associated with Rh-Cl is accompanied by a smaller peak which can be assigned to a Rh…Rh distance of 3.11 Å (phase corrected) (see Figure 6, for example). This distance is similar to that in the dinuclear species, $[Rh_2Cl_9]^{3-}$.[27] Extraction of this species has not been previously observed using **L2**, most likely because the earlier studies used lower concentrations of Rh.[13] That said, the presence of assemblies containing $[Rh_2Cl_9]^{3-}$ in extractions using other reagents has been reported, and can be attributed to different extraction conditions;[28] also, the DFT calculations of Samuels *et al.* predict that $[Rh_2Cl_9]^{3-}$ can be present in aqueous feed solutions.[7]

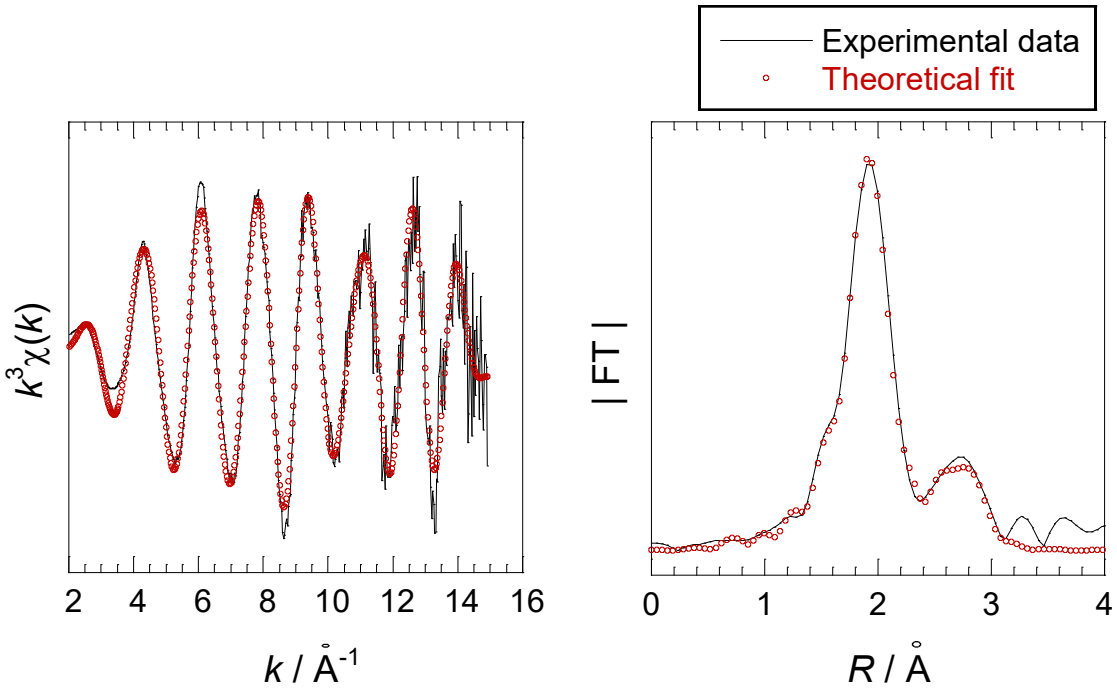

Figure 6. EXAFS (fluorescence mode) spectrum (phase shifts are not corrected) of sample (i), a $CDCl_3$ solution of **L2** after precontact with 2 M HCl and five contacts with an aqueous solution of Na_3RhCl_6 (0.1 M in 2.0 M HCl) (spectrum recorded ca. 1 month after phase separation).

^{1}H-^{15}N and ^{1}H-^{13}C NMR spectroscopy. The 2D ^{1}H-^{15}N HMBC spectrum of a $CDCl_3$ solution of **L2** is shown in Figure 7(a), together with those obtained after contact with aqueous 2 M HCl (b) and five contacts with 0.1 M Rh(III) in 2M HCl (c). As expected, protonation of the amine nitrogen atom is accompanied by a major shift in the ^{15}N signal (from 35.2 ppm in **L2** to 51.7 ppm in **L2**H·Cl and to 52.2 ppm in $[RhCl_5(H_2O)](\mathbf{L2}H)_2$, see Table 2). The spectra of the protonated extractant and the Rh-complex are very similar, suggesting both adopt a similar configuration and only weak ion-pairing interactions occur with the counter anions Cl^- and $[RhCl_5(H_2O)]^{2-}$. A much larger shift in the ^{15}N signal for the amide group would be expected if the ligand entered into the inner coordination sphere to form a complex similar to *fac*-[$RhCl_3$(**L4**)] (shown in Figure 4).

Spectrum (c) in Figure 7 also contains smaller resonances at ~128.9 and 130.7 ppm (labelled amide b), which have weak correlations with H-atoms 8 and 9. As the Rh-loaded sample was left for four months before the spectrum was recorded, it is possible that an inner sphere complex similar to *fac*-[$RhCl_3$(**L4**)] could have formed. If this were the case, we would expect to find a second amine ^{15}N resonance. We could find no evidence for a second resonance, indicating that inner sphere binding is unlikely, unless the resonance falls out with the range 50 to -150 ppm investigated here. Another

possible complication is that the high Rh(III) concentrations required for maximum loading into the organic phase result in the formation of $[Rh_2Cl_9]^-$·(**L2**H)$_3$ assemblies. However, if these are also outer sphere complexes, it is unlikely that ^{1}H, ^{13}C and ^{15}N NMR spectroscopy will be able to shed further light on this process.

The ^{1}H-^{13}C HMBC spectra (see Supporting Information) lead to the same conclusion as the ^{1}H-^{15}N spectra: the protonated form of **L2** in its HCl salt, and in the assemblies it forms when rhodium is extracted into $CDCl_3$, adopt a very similar structure and form only weak outer sphere interactions with chloridoaquo-Rh(III) complexes. This result is consistent with the data obtained by FT-IR spectroscopy, and the evidence from slope analysis (Figure 2) and EXAFS, which both indicate the prevalence of the $[RhCl_5(H_2O)]^{2-}$ anion.

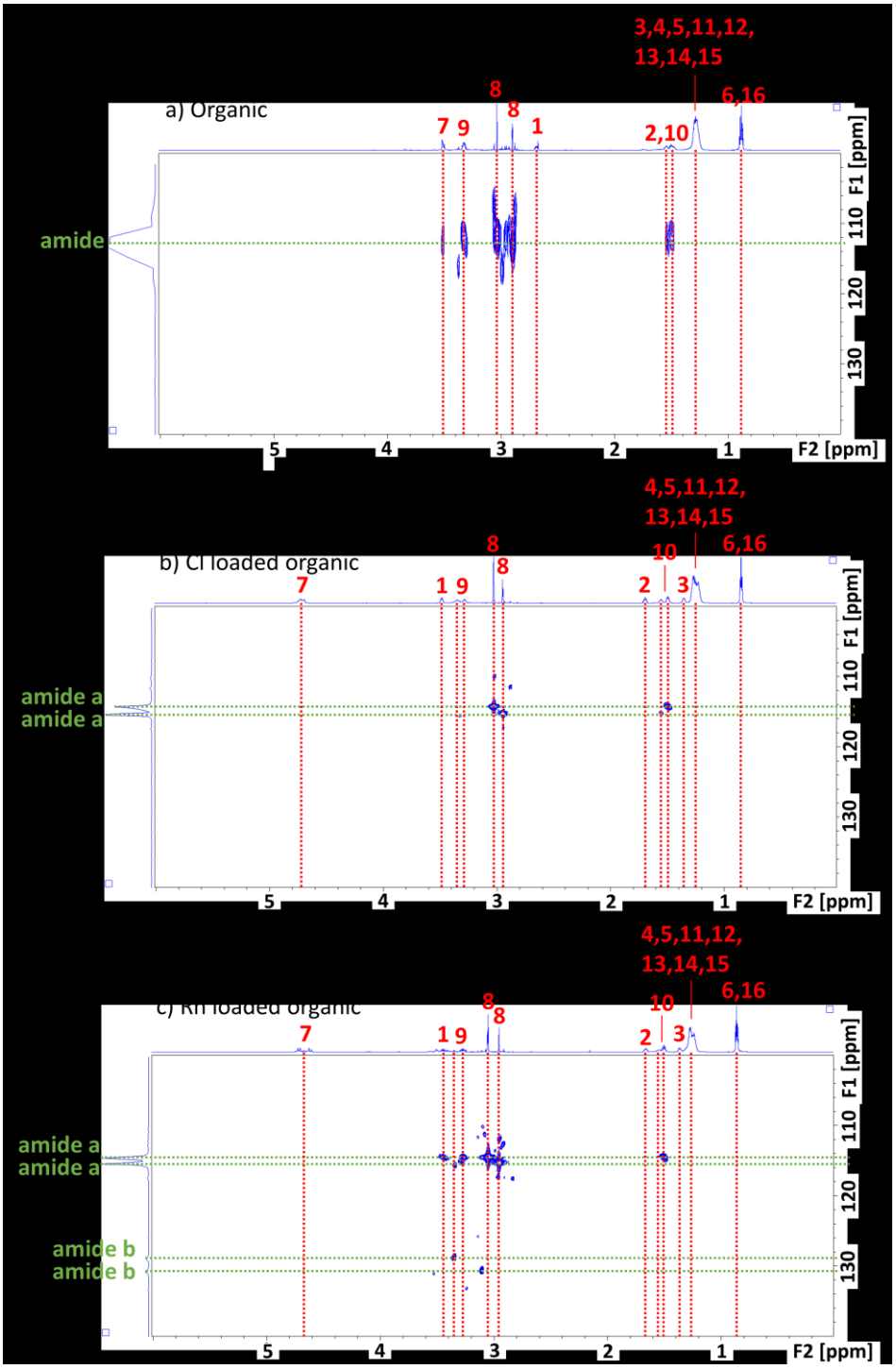
a) Organic
3,4,5,11,12,
13,14,15
6,16
8
8
7 9
1
2,10
amide
F1 [ppm]
110
120
130
5
4
3
2
1
F2 [ppm]
b) Cl loaded organic
4,5,11,12,
13,14,15
10
amide a
amide a
c) Rh loaded organic
amide b
amide b

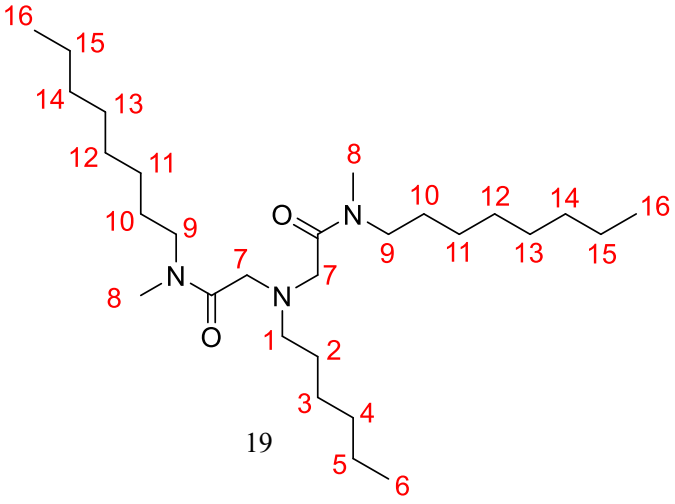
16
15
14
13
12
11
10
9
8
7
O
N
O
N
1
2
3
4
5
6
8
10
12
14
16
9
11
13
15

Figure 7. 2D ^{1}H-^{15}N HMBC spectra (^{1}H 0-6 ppm and ^{15}N 100-140 ppm) of a $CDCl_3$ solution of (a) **L2** (0.1 M), (b) **L2** (0.1 M) after contacting with 2 M HCl and (c) **L2** (0.1 M) after five contacts with aqueous Na_3RhCl_6 (0.1 M) in 2 M HCl to maximise Rh loading. Atom labels as shown on structure at bottom of figure.

Table 2. ^{15}N shifts (ppm) for amine and amide N atoms in the spectra shown in (a)-(c**)** in Figure 7. Full table (labelled and assigned cross-peaks) in the SI.

Spectrum		Amine	Amide	Amide	Amide	Amide
(a) **L2**	^{15}N shift / ppm	35.2	112.1	-	-	-
	Cross-peak…	1	2,7,8,9,10	-	-	-
(b) **L2**HCl	^{15}N shift / ppm	51.7	114.1	115.2	-	-
	Cross-peak…	1†,2	8,10	8,9*,10	-	-
(c) $[RhCl_5(H_2O)](\mathbf{L2}H)_2$	^{15}N shift / ppm	52.2	114.5	115.4	128.9	130.7
	Cross-peak…	2,7,8*	1,8,9,10	8,9*	9$^{\#}$	8$^{\#}$

*Weak or very weak cross-peaks.

$^{\#}$Cross-peak with region of H-peaks, but potentially not the same H-signal

†Not visible at peak intensity level displayed in spectra

Water transfer. The changes in the concentration of water in 1-octanol as Rh is taken up by **L2**H·Cl or **toa**H·Cl were determined by Karl Fisher titrations. The values recorded on the vertical axis in Figure 8 have been corrected for the baseline concentration of water in 1-octanol after it has been in contact with water alone and the concentration of water associated with $[RhCl_5(H_2O)]^{2-}$, which can be assumed to be the dominant Rh-species transferred from the aqueous phase (see above). In the absence of Rh(III), 0.50 M **L2**·HCl and 1.0 M **toa**H·Cl extract approximately 2.5 M and 1.5 M water. For both systems, the water content decreases as Rh is loaded. This is consistent with Rh(III) uptake involving the exchange of two chloride ions by $[RhCl_5(H_2O)]^{2-}$ (Equation 3). As the "hard" (charge dense) Cl^- ion will be more highly hydrated than the "softer" (charge diffuse) $[RhCl_5(H_2O)]^{2-}$ ion, the process will be associated with transfer of water molecules to the aqueous phase.

$$[RhCl_5(H_2O)]^{2-} + 2\mathbf{L}H{\cdot}Cl_{(org)} \rightleftharpoons [RhCl_5(H_2O)]{\cdot}(\mathbf{L}H)_{2(org)} + 2Cl^- \qquad \text{Equation 3}$$

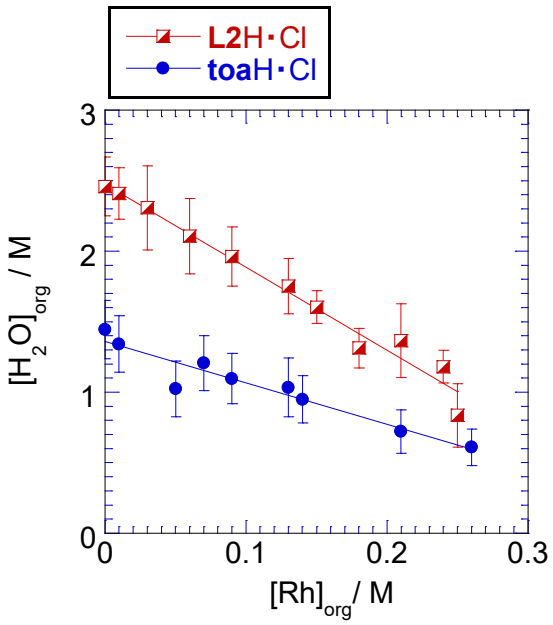

Figure 8. The decrease in water concentration in 1-octanol with uptake of $[RhCl_5(H_2O)]^{2-}$ by 0.5 M **L2**H·Cl or by 1.0 M **toa**H·Cl. The error bars represent 1σ.

SANS. The SANS profiles used to investigate the microscopic structures formed in 1–octanol by **L2** and **toa** are shown in Figure 9. Corrections for the scattering contributions from octanol-d_{17} have been made to all the profiles and the plots for the Rh-loaded solutions have been corrected for the contributions expected from the unloaded extractants present in the forms **L2**D·Cl and **toaD**·Cl (see plots in Figure 9).

The best-fit curves for the SANS profiles for **L2** were obtained using the hard-sphere model, with optimized solute structures provided by DFT calculations[14] (see Supporting Information), with the radii varying slightly from 9.7 ± 1.3 Å for (**L2**D·Cl)$_2$ to 10.9 ± 1.5 Å for $[RhCl_5(H_2O)]\cdot$(**L2**D)$_2$. The values of aggregation number, N_{agg}, which were evaluated from the forward scattering intensity, $I(q = 0$ Å$^{-1})$ (see Equation 9 in the Supporting Information), for **L2** and **L2**D·Cl in octanol-d_{17} lie in the range from 2 to 3, indicating the formation of dimeric and trimeric aggregates. The formation of an aggregate of **L2** is consistent with the shift of the $\nu_{C=O}$ stretching frequency in the FT-IR spectrum to a slightly lower frequency on dissolution in 1-octanol [see Figure 3, sample (b)]. **L2**DCl forms a well-defined dimer (N_{agg} = 2.1). The relative sizes and aggregation numbers recorded in Figure 9 are compatible with the water content of the organic phases as determined by the Karl Fischer titrations (see Figure 8). They support a Rh-loading mechanism in which three water molecules and two chloride ions in the dimeric $\{[$**L2**H·Cl$]_2.3(H_2O)\}$ are displaced by the $[RhCl_5(H_2O)]^{2-}$ dianion. A very different behavior is observed for **toa**, where much higher aggregation numbers are recorded for both

toa and **toa**D·Cl and a major rearrangement of the structures in solution accompanies the uptake of Rh giving a species with N_{agg} = 2.0 (Figure 9).

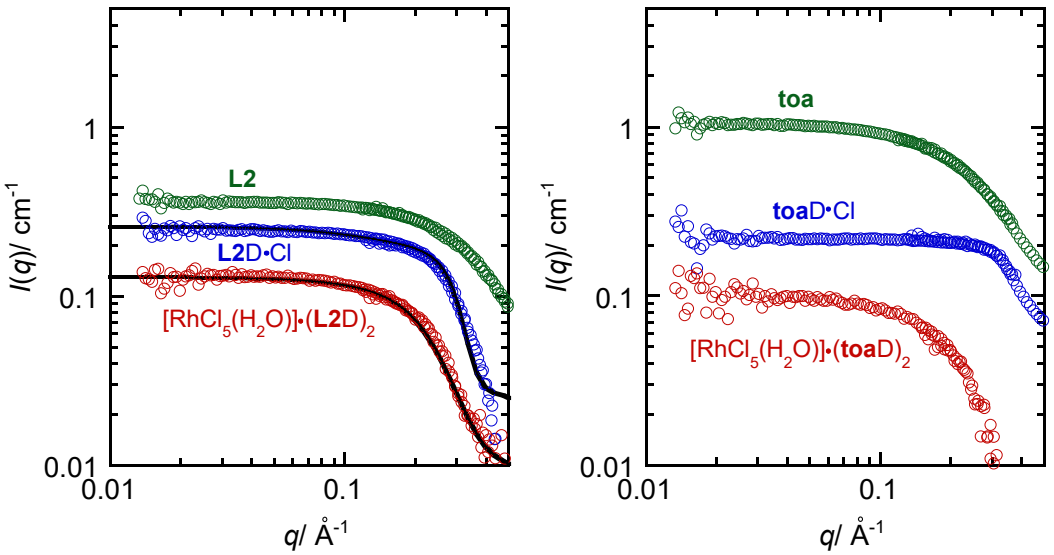

Sample	**L2**	**L2**D·Cl	$[RhCl_5(H_2O)]\cdot(\mathbf{L2}D)_2$
N_{agg}	2.7	2.1	1.1
Sample	**toa**	**toa**D·Cl	$[RhCl_5(H_2O)]\cdot(\mathbf{toa}D)_2$
N_{agg}	22.2	7.5	2.0

Figure 9. SANS profiles for 1-octanol-d_{17} solutions of (on the left): **L2**, **L2**D·Cl and $[RhCl_5(H_2O)](\mathbf{L2}D)_2$ and (on the right): **toa**, **toa**D·Cl and $[RhCl_5(H_2O)]\cdot(\mathbf{toa}D)_2$. Solid black curves are the best-fits obtained from a hard-sphere model with the optimized solute structures obtained by DFT calculation. Aggregation numbers for the same samples are summarized in the inset table.

Electrospray ionisation mass spectrometry (ESI-MS): Positive ion spectra of loaded organic phases obtained after extraction from aqueous solutions with different Rh concentrations are displayed in Figure 10. The dominant peak can be assigned to $[(\mathbf{L2}H)_3(RhCl_5)]^+$, m/z 1685.16. If this species arises from the extraction of $[RhCl_5(H_2O)]^{2-}$, the replacement of the *aquo* ligand might be associated with the age of the sample (48 hours). However, when ESI-MS was conducted on the organic phase within 5 minutes of very short contacts with the aqueous Rh-feed (<1 min, see Supporting Information) the $[(\mathbf{L2}H)_3(RhCl_5)]^+$ ion is still the most intense peak, strongly suggesting that changes to the inner coordination sphere must take place during ionization in the mass spectrometer.

After setting aside a sample (c) for seven months the dominant peak became m/z 1147.72 (see Figure 10), corresponding to $[(\mathbf{L2}H)(RhCl_3(\mathbf{L2}))]^+$. This peak most probably arises from the presence of the inner sphere complex $[RhCl_3(\mathbf{L2})]$ akin to the crystal structure of the model compound $[RhCl_3(\mathbf{L4})]$ (see Figure 4). This has important practical consequences for the use of **L2** in Rh-recovery by solvent extraction: for the short contact times and immediate stripping preferred in commercial solvent extraction circuits only $[RhCl_5(H_2O)]^{2-}$ will be recovered.

When aqueous solutions with high Rh concentrations were used in loading experiments, a peak in the positive ion ESI-MS was found at m/z 2398.46, which corresponds to $[(\mathbf{L2}H)_4(Rh_2Cl_9)]^+$. A dinuclear species with a Rh…Rh separation of 3.11 Å was also found in the EXAFS studies (see above). Other species identified in the spectra of extracts from aqueous solutions of high Rh concentrations, which likely indicates the presence of dinuclear Rh complexes, are discussed in the Supporting Information.

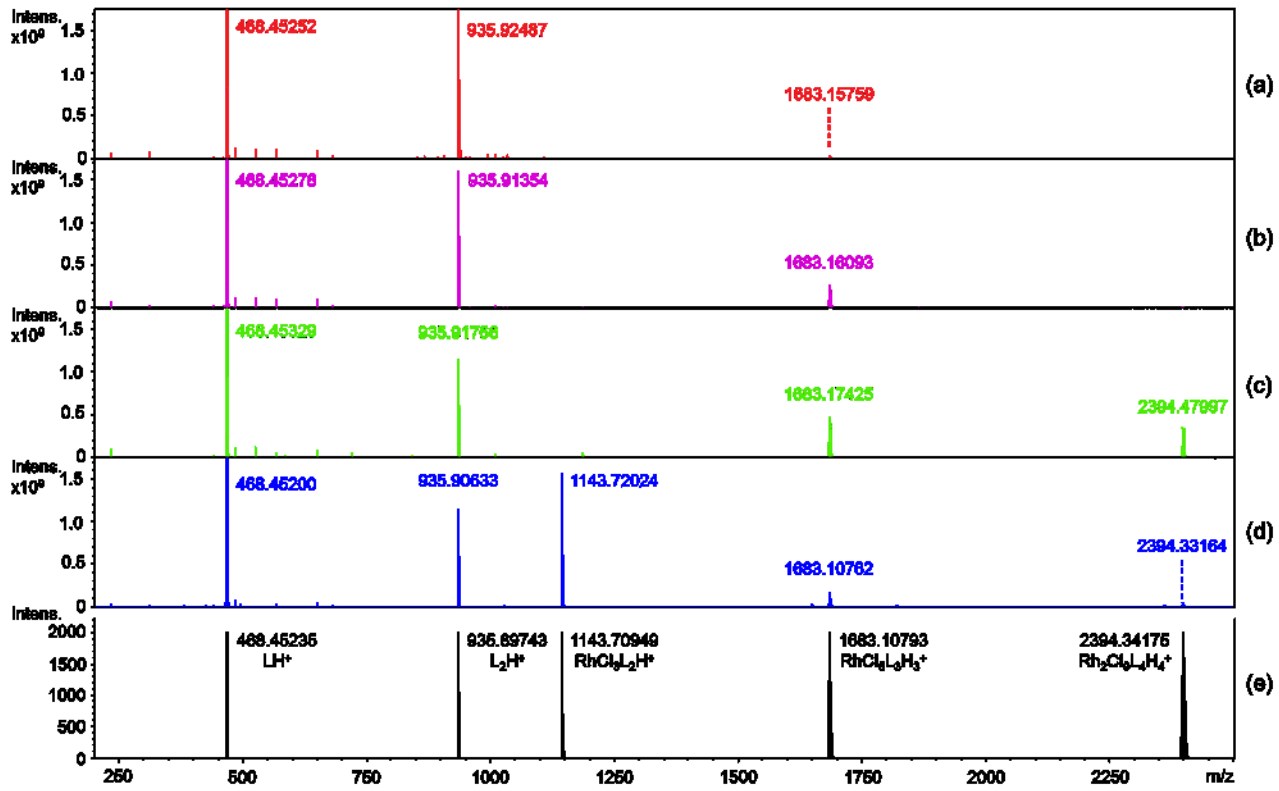

Figure 10. Positive ion ESI-MS of Rh(III)-loaded $CHCl_3$ solutions of 0.5 M **L2**. Samples (a)-(c) are from extractions from 0.001 M, 0.01 M, and 0.1 M Rh in 2 M HCl solutions, analysed 48 hours after extraction. Contrast with sample (d) which is (c) after ageing for 7 months. (e) provides the simulated spectra. Monoisotopic mass labelling given.

Computational modelling: Density Functional Theory (DFT) calculations were undertaken to define the most favourable structures of the assemblies [**L**H·Cl] and $[RhCl_5(H_2O)](\mathbf{L}H)_2$. Because large

numbers of energetically similar conformations exist for the *n*-hexyl and *n*-octyl groups on the extractants **L1**-**L3**, the truncated homologues, **L5**-**L7**, having only methyl substituents, were used as models to facilitate energy-minimisation. For **toa**, similar truncation to trimethylamine will not provide a realistic model for defining which polarised C-$H^{\delta+}$ units can make contacts with the anions. Consequently, for this system the untruncated extractant was used in the calculations.

The energy-minimised forms of these structures were then used to calculate the energies of the anion exchange reaction (Equation 7). As the SANS results suggested that **L2**H·Cl exists as a dimer in octanol, the anion-exchange reaction for the model compound **L6** starting from a dimer form (Equation 8) was also computed.

$$\mathbf{L}_{(org.)} + H_3O^+_{(aq.)} \rightleftharpoons \mathbf{L}H^+_{(org.)} + H_2O_{(aq.)} \quad \text{Equation 4}$$

$$\mathbf{L}H^+_{(org.)} + Cl^-_{(aq.)} \rightleftharpoons \mathbf{L}H{\cdot}Cl_{(org.)} \quad \text{Equation 5}$$

$$2\mathbf{L}H^+_{(org.)} + [RhCl_5(H_2O)]^{2-}_{(aq.)} \rightleftharpoons [RhCl_5(H_2O)]{\cdot}(\mathbf{L}H)_{2(org.)} \quad \text{Equation 6}$$

$$2\mathbf{L}H{\cdot}Cl_{(org.)} + [RhCl_5(H_2O)]^{2-}_{(aq.)} \rightleftharpoons [RhCl_5(H_2O)]{\cdot}(\mathbf{L}H)_{2(org.)} + 2Cl^-_{(aq.)} \quad \text{Equation 7}$$

$$(\mathbf{L}H{\cdot}Cl)_{2(org.)} + [RhCl_5(H_2O)]^{2-}_{(aq.)} \rightleftharpoons [RhCl_5(H_2O)]{\cdot}(\mathbf{L}H)_{2(org.)} + 2Cl^-_{(aq.)} \quad \text{Equation 8}$$

Work focused initially on identifying the site of protonation in the lowest energy forms of the cations **L5**H^+, **L6**H^+**,** **L7**$H^+$and **toa**H^+. As expected, the conformation of **toa**H^+ differs markedly from the protonated forms of the amidoamines. In **toa**H^+ the *n*-octyl groups bend away from the N-H^+ unit to minimise repulsion from methylene C-H units (Figure 11). In contrast, for the protonated amidoamines, the amide arms bend towards the N-H^+ unit to form proton chelate units of the type that have been discussed above. The structure of the diamido ligand **L6**H^+ is shown as an example in Figure 11; note the structure lacks symmetry as the two NH^+…O=C distances are slightly different (2.03 and 2.11 Å).

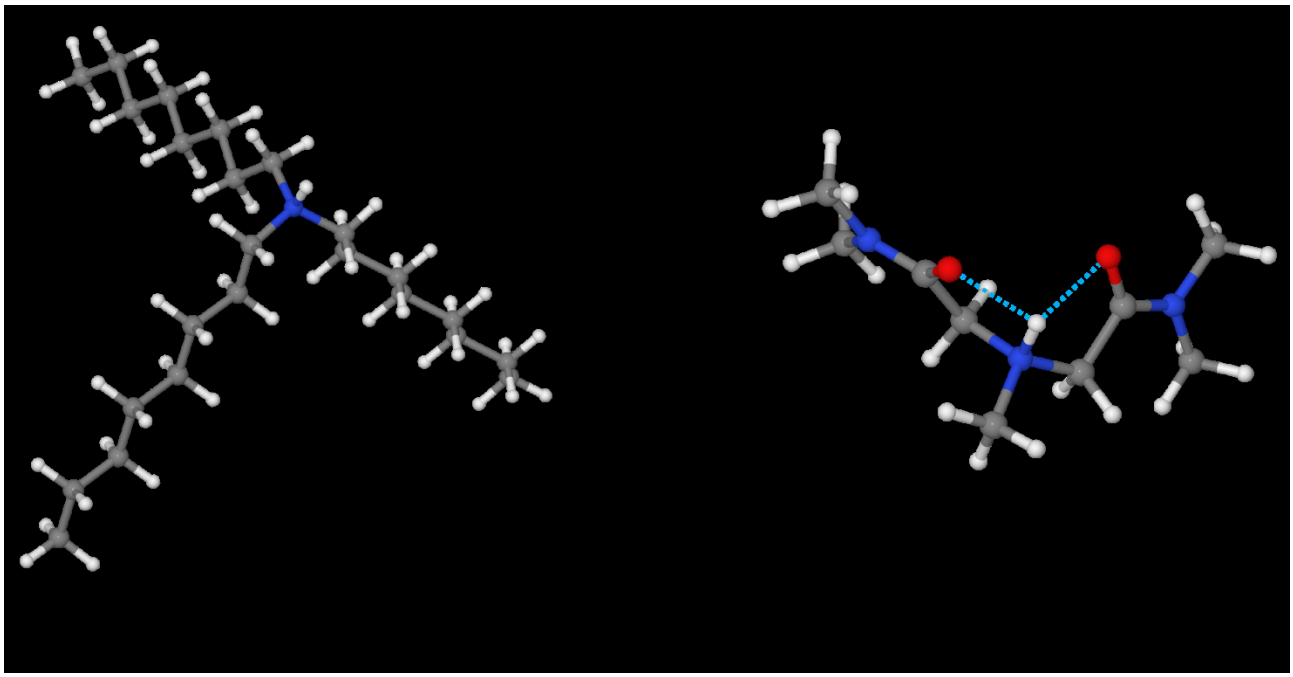

Figure 11. Optimised structures of (a) **toa**H^+ and (b) **L6**H^+.

Increasing the number of interactions between the N-H^+ group and amide oxygen atoms accounts for the basicity increasing in the order monoamide, **L5**H < diamide, **L6**H < triamide, **L7**H, as revealed by the calculated free energies for the reaction in Equation 4 (see Table 3).

Table 3. Free energy changes for the processes outlined in Equations 4-8.

Process	Ligand	ΔG/ kJ mol^{-1}
Equation 4	**L5**	-116.4
	L6	-117.5
	L7	-122.8
Equation. 5	**L5**	-22.5
	L6	-10.6
	L7	-2.9 #
Equation 6	**L5**	-18.2
	L6	-31.4
	L7	-14.1 #
Equation. 7	**L5**	26.8
	L6	-10.2
	L7	-8.2 #
Equation 8	**L5**	*
	L6	-6.8

	L7	*

[#] Energies were calculated using structures that failed to fully optimise – see Methods section for more details. [*] Not calculated

The potential chelation of the N-H^+ unit in the ligands has a major influence on the mode of binding to anions. The N-H^+ proton in the **L5**H^+ ligand makes close contact with Cl^- in the lowest energy forms of the ion pairs **L**H·Cl (see Figure 12) and chelation by an amide oxygen atom does not occur. In contrast, chelation of the proton by more than one amide oxygen atom templates **L6**H^+ and **L7**H^+ such that the proton is more centrally located in the superstructure and an array of polarised C-$H^{\delta+}$ units is provided on the opposite side of the ligands from the amide oxygen atoms. As a consequence, the lowest energy forms of the ion pairs **L6**H·Cl and **L7**H·Cl (Figure 12) has no direct N-H^+…Cl interaction and, instead, several weakly bonding C-$H^{\delta+}$…Cl^- interactions are formed. DFT calculations confirm that the energy-minimized form of the dimer is more stable than the monomer by 7.6 kJ mol^{-1}.

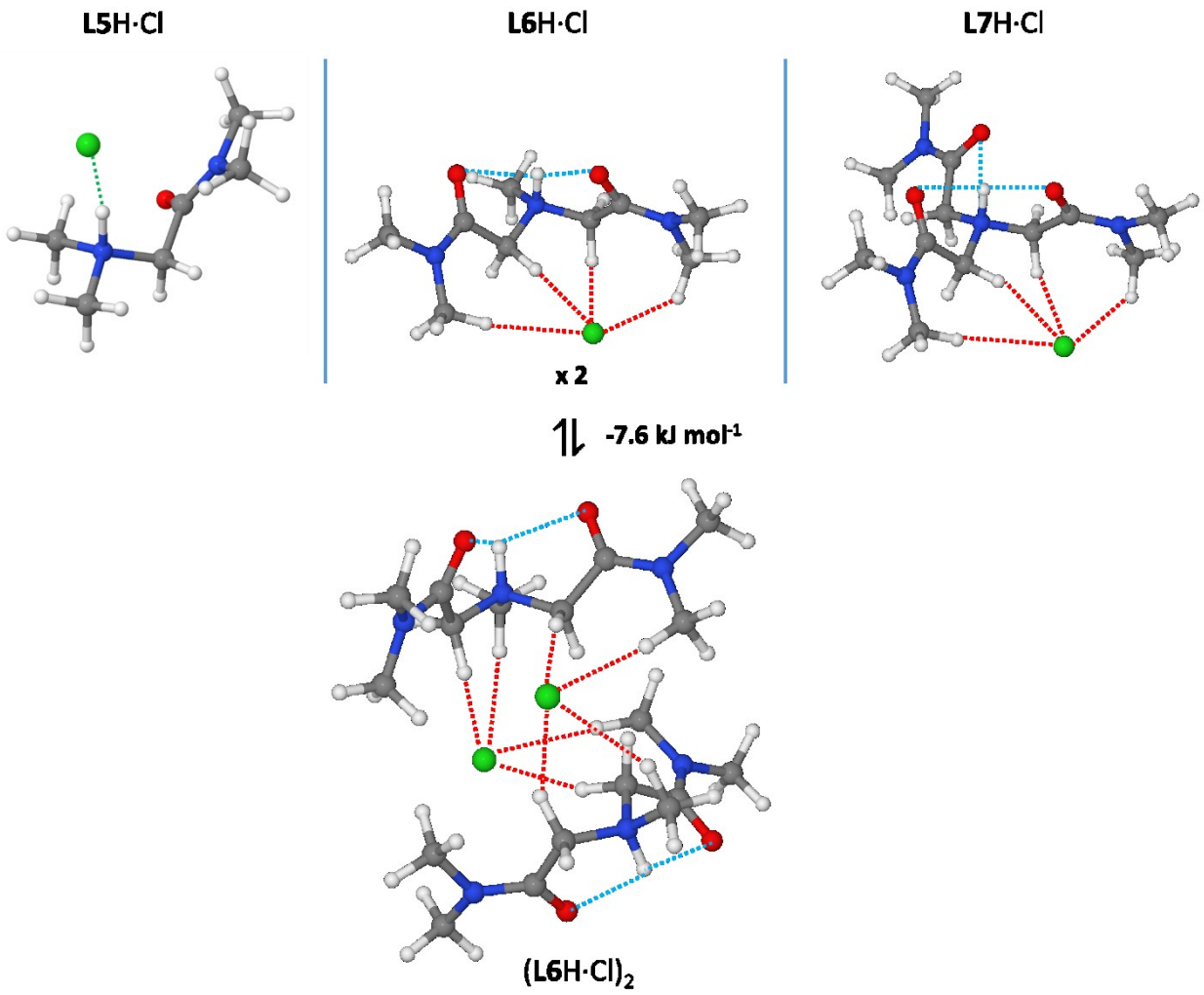

Figure 12. The lowest energy structures of the ion pairs formed with Cl^- (shown in green) by **L5**H^+, **L6**H^+ and **L7**H^+ and the dimer [**L6**H·Cl]$_2$. Hydrogen bonds involving the carbonyl oxygen atom are shown in blue and short contacts made by N-H and C-H hydrogen atoms to Cl^- in green and red, respectively.

For $[RhCl_5(H_2O)]^{2-}$, it is possible that the *aquo* ligand may act as a hydrogen-bond donor to an amide O atom in **L**. As such, different starting structures were used in the calculations (see Supporting Information) with arrangements in which either the *aquo* ligand approaches the amide oxygen atoms or the chloride ligands approach the C-$H^{\delta+}$ or N-H^+ groups (and assuming a proton chelate does or does not form, respectively). The lowest energy structures found for the $[RhCl_5(H_2O)]\cdot(\mathbf{L}H)_2$ assemblies are shown in Figure 13. Only **L5**H^+ gives an assembly in which the most stable form involves the formation of a hydrogen bond with the *aquo* ligand and in this assembly only one of the two cationic **L5**H^+ ligands functions in this way. The carbonyl group that is hydrogen bonded to the *aquo* ligand does not chelate to the N-H^+ group, presumably to ensure a higher partial negative charge on the O atom that acts as the hydrogen-bond acceptor. The free amido NH group makes close

contacts with the chloride ligands on the same face of the octahedral $[RhCl_5(H_2O)]^{2-}$ ion. The other **L5**H^+ ligand also has no C=O···HN^+ proton chelate and addresses the chloride ligands on the opposite face of the Rh(III) octahedron through a combination of N–H^+ and C–$H^{\delta+}$ groups. Structure (d) in Figure 13 displays the favorable N–H^+···Cl^- binding mode when the link to the *aquo* ligand is severed, but the overall structure is significantly less energetically favorable (by 15.3 kJ mol^{-1}) than structure (a).

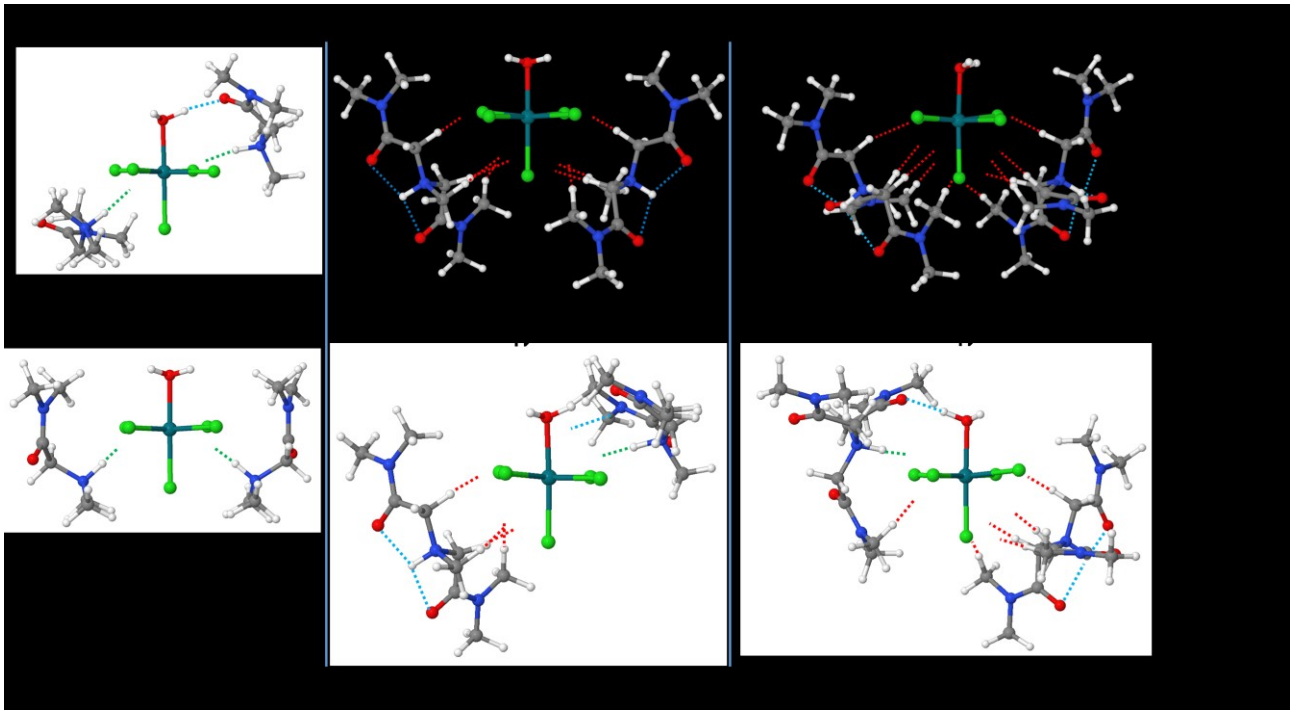

Figure 13. Structures of lowest energy forms of the assemblies $[RhCl_5(H_2O)]\cdot(\mathbf{L}H)_2$ formed by **L5**H^+, **L6**H^+ and **L7**H^+ (**a**, **b** and **c** respectively). Structures **d**, **e** and **f** are the next energetically favourable forms with an alternative binding mode, with only **L5**H^+ making close contacts with the chloride ligands (**d**) and with **L6**H^+ and L7H^+ forming an H-bond with the *aquo* ligand. Hydrogen bonds involving carbonyl oxygen atom are shown in blue and those involving N-H and C-H hydrogen atoms to chloride ions or the edges or faces of the octahedron in green and red, respectively. *Energy for structure (f) used in energy difference calculation from structure which had not fully optimised (see Experimental section for details).

The preferred binding modes of the protonated forms of the diamide **L6** and the triamide **L7** differ markedly from those of **L5.** The lowest energy structures of both $[RhCl_5(H_2O)]\cdot(\mathbf{L6}H)_2$ and $[RhCl_5(H_2O)]\cdot(\mathbf{L7}H)_2$ contain the proton-chelated form of the cations [see Figure 13, (b) and (c)] and use only C-$H^{\delta+}$ groups to make bonding contacts to the anion. Neither contain hydrogen bonds involving the *aquo* ligand. The lowest energy form of $[RhCl_5(H_2O)]\cdot(\mathbf{L6}H)_2$ that has an O-H···O=C

hydrogen bond [see (e) in Figure 13] is 16.9 kJ mol^{-1} less stable than structure (b). The **L6**H^+ unit which forms this hydrogen bond also forms a bonding contact between its NH^+ group and a chloride ligand. The other **L6**H^+ ligand is bound in a similar manner to that in the lowest energy form [(b) in Figure 13]. Similar behaviour is observed with the triamide **L7**. Similar mechanisms involving C-$H^{\delta+}$ groups to stabilise anions in aqueous environments have been reported by others using NMR spectroscopy.[29]

It is of interest to consider whether the calculated gas-phase energies of formation of the assemblies $[RhCl_5(H_2O)]\cdot(\mathbf{L}H)_2$ correlate with the observed relative strengths of the amidoamine extractants. Models for assemblies formed by **toa**H^+ were excluded from this analysis because the experimental data gleaned from the SANS measurements indicate that the mode of action for this extractant is very different, and computing the large assemblies of **toa** and **toa**H^+ that exist in solution prior to formation of complexes with $[RhCl_5(H_2O)]^{2-}$ and Cl^- would require a different approach from the DFT modelling undertaken here; classical molecular dynamics modelling, such as carried out by MacRuary *et al.* to investigate the assemblies formed in the extraction of $PtCl_6^{2-}$ and chloride by **tbp** (tributylphosphate) would be more appropriate.[30] The data presented in Table 3 for the exchange reaction in Equation 7 (or Equation 8, assuming a dimer structure for **L6**) are consistent with the selectivity for $[RhCl_5(H_2O)]^{2-}$ over Cl^-, varying in the order triamide **L7**H^+ ≈ diamide **L6**H^+ >> monoamide **L5**H^+. This is the same order as that observed for the strengths of the equivalent hydrophobic extractants (triamide **L3**H^+ ≈ diamide **L2**H^+ >> monoamide **L1**H^+) for Rh-loading into chloroform.[13b] As there is a large excess of chloride in the aqueous feeds, the *strengths* observed experimentally will be very dependent on the *selectivity* for $[RhCl_5(H_2O)]^{2-}$ over Cl^-. The data in Table 3 suggest that this selectivity arises because the binding energy to Cl^- (Equation 5) is highest for the monoamide **L5**H^+ while, conversely, the binding energies to $[RhCl_5(H_2O)]^{2-}$ (Equation 6) are significantly higher for the di- and triamides **L6**H^+ and **L7**H^+. This increasing strength of binding to $[RhCl_5(H_2O)]^{2-}$ arises due to ligand preorganization upon protonation, which provides a cavity of polarised C-$H^{\delta+}$ groups over which the positive charge is diffusely spread, that together presents an excellent binding site for three chloride ligands of the charge diffuse $[RhCl_5(H_2O)]^{2-}$ anion. This cavity in **L6**$H^+$is shown in the upper part of Figure 14, and accounts for the striking increase in selectivity and strength of the related extractants **L2** and **L3** over the monoamide **L1**.

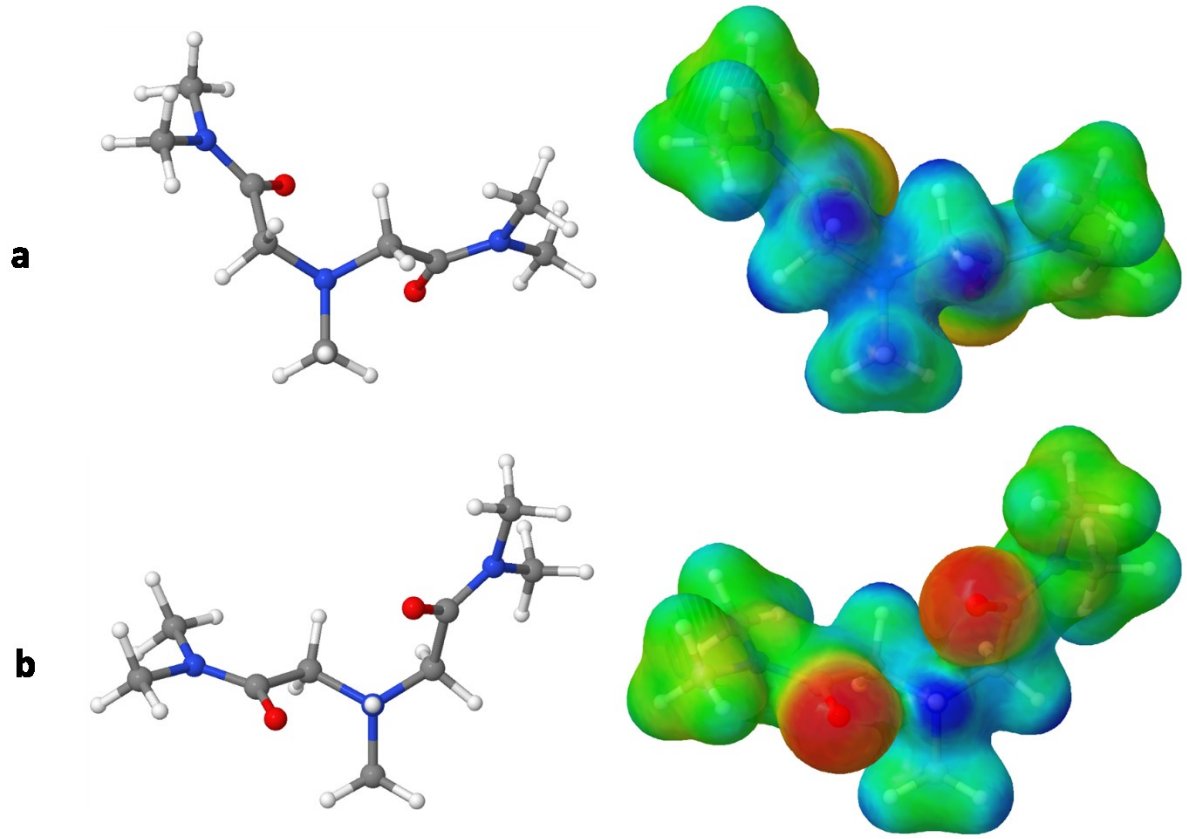

Figure 14. Two views of **L6**H^+ and its associated electrostatic potential plot. The cavity of polarised C-$H^{\delta+}$ groups is shown in (a) and the proton chelated units in (b) (blue and red areas indicate relative positive and negative charge, respectively).

Finally, the EXAFS and ESI-MS experiments suggest that the use of high concentrations of Rh and/or a low extractant to Rh ratio with **L2** leads to the formation of assemblies containing the dinuclear species, $[Rh_2Cl_9]^{3-}$. Calculations show that **L6**H^+ can form the neutral assembly $[Rh_2Cl_9]\cdot(\mathbf{L6}H)_3$ (see Figure 15) in which the ligands provide a polarised C-$H^{\delta+}$ cavity similar to that in Figure 13(b) which can also accommodate the chloridoaquo-metalate bridging chloride atoms.

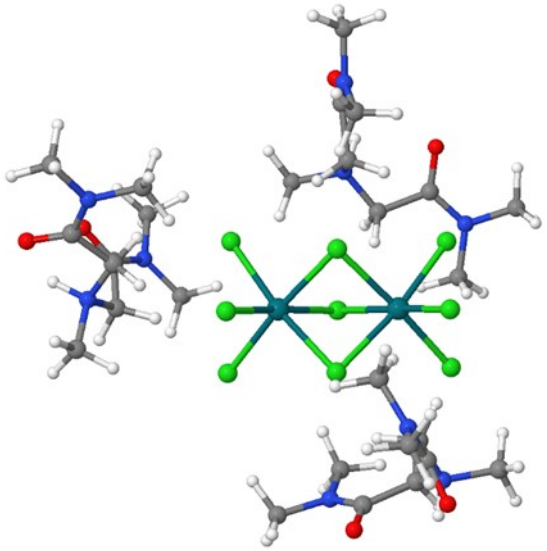

Figure 15. Structure of the lowest energy form of $[Rh_2Cl_9]\cdot(\mathbf{L6}H)_3$.

Conclusions

Solvent extraction offers promise to improve on current practices for the recovery of rhodium, but the presence of mixed speciation states following acid chloride leaching complicates the chemical separation stage. Herein we have shown that Rh(III) extraction data, characterized by slope analysis, FT-IR, EXAFS, ESI-MS, NMR and SANS point towards the dianion $[RhCl_5(H_2O)]^{2-}$ being transferred to the organic phase in a process which involves formation of an outer-sphere assembly with the diamidoamine reagent N-n-hexyl-bis(N-methyl-N-n-octyl-ethylamide)amine (**L2**); $[RhCl_5(H_2O)]\cdot(\mathbf{L2}H)_2$. We have shown that it is possible to prepare inner-sphere complexes such as $[RhCl_3(\mathbf{L2})]$ but only by using forcing conditions in a single phase or by ageing solutions from solvent extraction experiments. As the outer-sphere complex is kinetically labile, loading, and subsequent stripping, of the metal from the organic phases should be obtainable with short contact times; indeed, maximum Rh uptake was observed within 10 minute contact times, the shortest used in this work. ESI-MS and EXAFS measurements have also shown that $[Rh_2Cl_9]^{3-}$ is extracted at high Rh(III) concentrations.

The amidoamine reagents **L1-L3** used in this work are proton chelating ligands. DFT calculations on model compounds show that the addition of a proton sets up an internal hydrogen bond which pre-organizes the ligand to present a charge diffuse cavity of polarized $C\text{-}H^{\delta+}$ groups to interact with the chloride ligands on the octahedral faces of the charge-diffuse $[RhCl_5(H_2O)]^{2-}$ dianion. This binding

arrangement is more thermodynamically favorable than the N-$H^{\delta+}$ binding to the competitor anion Cl^-, which is present in vast excess in acid chloride media. In this way selectivity for Rh(III) over Cl^- has been achieved.

The mechanism of extraction by the amido-extractants **L1-L3** differs markedly from that by **toa.** The higher level of aggregation of **toa** and **toa**H·Cl in 1-octanol, as detected by SANS, means that substantial reorganisation is required to generate the $[RhCl_5(H_2O)]\cdot(\mathbf{toa}H)_2$ assembly formed on Rh-extraction. This is the likely reason for **toa** being an inferior extractant for Rh(III).

For the most studied extractant, **L2**, we have found no experimental evidence for the carbonyl oxygen atoms acting as hydrogen-bond acceptors from the *aquo* ligand in $[RhCl_5(H_2O)]^{2-}$. This is consistent with the computed lowest energy structures of the $[RhCl_5(H_2O)]\cdot(\mathbf{L}H)_2$ assemblies formed by the *di-* and *tri*-amido models, **L6** and **L7**, where carbonyl groups chelate the proton of the N–H^+ group, restricting their accessibility to the *aquo* ligand. The situation is different for the mono-amide, **L5**H^+, where the absence of the proton chelate facilitates formation of a classical N-H^+···O=C hydrogen bond.

The reduced propensity for **L5**H^+ to favor a proton-chelated structure compared with the *di-* and *tri*-amides **L6**H^+ and **L7**H^+ also helps to explain why it more readily rearranges to make the N–H^+ group accessible to Cl^- in the **L**H·Cl ion pair. As a consequence, the selectivity for binding to $[RhCl_5(H_2O)]^{2-}$ over Cl^- will be greatly reduced, thus helping to account for **L2** and **L3** being stronger Rh-extractants than the monoamide **L1**. For the amidoamine extractants **L1-L3** the correlation between the observed order of strengths Rh-loading into chloroform extractants (triamide **L3**H^+ ≥ diamide **L2**H^+ >> monoamide **L1**H^+)[13b] and the calculated energies for formation via the gas phase exchange reaction models **L5-L7 (**triamide **L7**H^+ ≈ diamide **L6**H^+ >> monoamide **L5**H^+) is remarkable.

Despite the complexity associated with the aqueous feeds containing a mixture of chloridoaquo-Rh(III) complexes and the most predominant of these, $[RhCl_5(H_2O)]^{2-}$, having both hydrogen-bond acceptor and donor groups, extraction by **L1-L3** follows the behavior of other amidoamine reagents when loading symmetrical chloridometalates, MCl_x^{y-}. Extraction efficiency follows the Hofmeister bias[31] which predicts that dianionic metallates will be extracted preferentially over trianionic analogues as a consequence of their lower hydration energies. This contributes to $[RhCl_5(H_2O)]^{2-}$ being extracted more readily than $[RhCl_6]^{3-}$. The greater uptake of Pt and Pd compared to Rh by **L1-L3**[13] (highlighted in the Supporting Information) is consistent with the higher hydration energy of $[RhCl_5(H_2O)]^{2-}$ compared to $[PtCl_6]^{2-}$ and $[PdCl_4]^{2-}$ that is conferred by the *aquo* ligand.

Acknowledgements

We thank Ms. Hiroko Niiyama (AIST) for her technical assistance and Dr. Takeshi Kawasaki (Toho University) for helpful discussions on the XRD analysis. Part of this study was performed under the Shared Use Program of JAEA Facilities (proposal nos. 2015A-E07 and 2015B-E08) supported by JAEA Advanced Characterization Nanotechnology Platform as a program of "Nanotechnology Platform" of the Ministry of Education, Culture, Sports, Science and Technology (MEXT), Japan. The synchrotron radiation experiments were performed on JAEA beamline BL11XU at SPring-8 (proposal nos. 2015A3517 and 2015B3518). We thank Dr. Juraj Bella (University of Edinburgh) for recording the ^{1}H, ^{1}H-^{1}H COSY, ^{13}C, ^{1}H-^{13}C HMBC, and ^{1}H-^{15}N HMBC NMR spectra and Dr. Logan MacKay for helpful discussions on ESI-MS. We thank the Diamond Light Source for on the data collected on Beamline B18 (Rapid Access Proposal SP15757). We also acknowledge the University of Edinburgh ECDF and EaStCHEM Research Computing Facility for hardware and software access, respectively. M.A. acknowledges the support of the U.S. Department of Energy (DOE), Office of Science, Office of Basic Energy Sciences, Chemical Sciences, Geosciences, and Biosciences Division, under contract no. DE-AC02-06CH11357. A portion of this research used resources at the Spallation Neutron Source, a DOE Office of Science User Facility operated by the Oak Ridge National Laboratory.

Supporting Information. Reagents and synthesis; Sample preparation for FT-IR, EXAFS, Karl Fisher and SANS measurements; SANS sample properties; Calculations of SANS profiles; data collection and analysis for EXAFS, NMR spectroscopy, ESI-MS spectrometry; crystal data and structure determination for **L4** and [$RhCl_3$(**L4**)]·$4CHCl_3$; Details of computational modelling simulations; Comparison of extraction of Rh(III), Pd(II) and Pt(IV) by **L1**, **L2** and **L3**.

REFERENCES

1. (a) Nelson, J. J. M.; Schelter, E. J., Sustainable Inorganic Chemistry: Metal Separations for Recycling. *Inorganic Chemistry* **2019,** *58* (2), 979-990; (b) Cheisson, T.; Schelter, E. J., Rare earth

elements: Mendeleev's bane, modern marvels. *Science* **2019,** *363* (6426), 489.

2. Greenfield, A.; Graedel, T. E., *The omnivorous diet of modern technology*. 2013; Vol. 74, p 1-7.

3. Nuss, P.; Eckelman, M. J., Life Cycle Assessment of Metals: A Scientific Synthesis. *PLOS ONE* **2014,** *9* (7), e101298.

4. Graedel, T. E.; Allwood, J.; Birat, J. P.; Buchert, M.; Hageluken, C.; Reck, B. K.; Sibley, S. F.; Sonnemann, G., What do we know about metal recycling rates? *Journal of Industrial Ecology* **2011,** *15* (3), 355-366.

5. Wilson, A. M.; Bailey, P. J.; Tasker, P. A.; Turkington, J. R.; Grant, R. A.; Love, J. B., Solvent extraction: the coordination chemistry behind extractive metallurgy. *Chemical Society Reviews* **2014,** *43* (1), 123-134.

6. Benguerel, E.; Demopoulos, G. P.; Harris, G. B., Speciation and separation of rhodium(III) from chloride solutions: a critical review. *Hydrometallurgy* **1996,** *40* (1-2), 135-52.

7. Samuels, A. C.; Boele, C. A.; Bennett, K. T.; Clark, S. B.; Wall, N. A.; Clark, A. E., Integrated Computational and Experimental Protocol for Understanding Rh(III) Speciation in Hydrochloric and Nitric Acid Solutions. *Inorganic Chemistry* **2014,** *53* (23), 12315-12322.

8. Narita, H.; Tanaka, M.; Shiwaku, H.; Okamoto, Y.; Ikeda-Ohno, A.; Yaita, T., Inner-sphere structure of rhodium complexes with tin(II) chloride in concentrated hydrochloric acid solution. *Bulletin of the Chemical Society of Japan* **2013,** *86* (2), 203-209.

9. (a) Rydberg, J.; Cox, M.; Musikas, C.; Choppin, G. R., Solvent Extraction in Hydrometallurgy. In *Solvent Extraction Principles and Practice*, M., C., Ed. Elsevier: Oxford, 2004; pp 455-505; (b) Crundwell, F.; Moats, M.; Ramachandran, V.; Robinson, T.; Davemport, W. G., Refining of the platinum-group metals. In *Extractive Metallurgy of Nickel, Cobalt and Platinum Group Metals*, Amsterdam, 2011; pp 489-534; (c) Grant, R. A.; Woollam, S., The role of solvent extraction in platinum group metal refining – past, present and future. In *ISEC 2014*, Würzburg, Germany, 2014.

10. (a) Benguerel, E.; Demopoulos, G. P., Formation and extraction of Rh–Sn–Cl complexes with an alkylated 8-hydroxyquinoline. *Journal of Chemical Technology & Biotechnology* **1998,** *72* (2), 183-189; (b) Narita, H.; Tanaka, M.; Yaita, T.; Okamoto, Y., Extraction and structural propertiesd of rhodium-tin complexes in solution. *Solvent Extraction and Ion Exchange* **2004,** *22* (5), 853-863.

11. (a) Carson, I.; MacRuary, K. J.; Doidge, E. D.; Ellis, R. J.; Grant, R. A.; Gordon, R. J.; Love, J. B.; Morrison, C. A.; Nichol, G. S.; Tasker, P. A.; Wilson, A. M., Anion Receptor Design: Exploiting Outer-Sphere Coordination Chemistry To Obtain High Selectivity for Chloridometalates over Chloride. *Inorg. Chem.* **2015,** *54* (17), 8685-8692; (b) Maeda, M.; Narita, H.; Tokoro, C.; Tanaka, M.; Motokawa, R.; Shiwaku, H.; Yaita, T., Selective extraction of Pt(IV) over Fe(III) from HCl with an amide-containing tertiary amine compound. *Sep. Purif. Technol.* **2017,** *177*, 176-181; (c) Warr, R. J.; Bell, K. J.; Gadzhieva, A.; Cabot, R.; Ellis, R. J.; Chartres, J.; Henderson, D. K.; Lykourina, E.; Wilson, A. M.; Love, J. B.; Tasker, P. A.; Schröder, M., A Comparison of the Selectivity of Extraction of [PtCl6]2– by Mono-, Bi-, and Tripodal Receptors That Address Its Outer Coordination Sphere.

Inorganic Chemistry **2016,** *55* (12), 6247-6260; (d) Ellis, R. J.; Chartres, J.; Henderson, D. K.; Cabot, R.; Richardson, P. R.; White, F. J.; Schröder, M.; Turkington, J. R.; Tasker, P. A.; Sole, K. C., Design and Function of Pre-organised Outer-Sphere Amidopyridyl Extractants for Zinc(II) and Cobalt(II) Chlorometallates: The Role of C-H Hydrogen Bonds. *Chemistry – A European Journal* **2012,** *18* (25), 7715-7728; (e) Turkington, J. R.; Cocalia, V.; Kendall, K.; Morrison, C. A.; Richardson, P.; Sassi, T.; Tasker, P. A.; Bailey, P. J.; Sole, K. C., Outer-Sphere Coordination Chemistry: Amido-Ammonium Ligands as Highly Selective Tetrachloridozinc(II)ate Extractants. *Inorganic Chemistry* **2012,** *51* (23), 12805-12819; (f) Paiva, A. P., Recycling of Palladium from Spent Catalysts Using Solvent Extraction—Some Critical Points. *Metals* **2017,** *7* (11), 505; (g) Bélair, S.; Breeze, B.; O'Shaughnessy, P.; Schofield, E.; Grant, R.; Woollam, S., Separation of ruthenium, iridium and rhodium by solvent extraction using an amide extractant. In *ISEC 2011*, Santiago, Chile, 2011.

12. Bowen, S. M.; Duesler, E. N.; Paine, R. T., Synthesis and crystal and molecular structures of diisopropyl N,N-diethylcarbamylmethylenephosphonate samarium nitrate and erbium nitrate complexes. *Inorganica Chimica Acta* **1982,** *61*, 155-166.

13. (a) Narita, H.; Morisaku, K.; Tanaka, M., The first effective extractant for trivalent rhodium in hydrochloric acid solution. *Chem. Commun. (Cambridge, U. K.)* **2008,** *45* (45), 5921-5923; (b) Narita, H.; Morisaku, K.; Tanaka, M., Highly Efficient Extraction of Rhodium(III) from Hydrochloric Acid Solution with Amide-Containing Tertiary Amine Compounds. *Solvent Extr. Ion Exch.* **2015,** *33* (4), 407-417.

14. Motokawa, R.; Kobayashi, T.; Endo, H.; Mu, J.; Williams, C. D.; Masters, A. J.; Antonio, M. R.; Heller, W. T.; Nagao, M., A Telescoping View of Solute Architectures in a Complex Fluid System. *ACS Central Science* **2019,** *5* (1), 85-96.

15. Sheldrick, G. M., Crystal structure refinement with SHELXL. *Acta Crystallogr., Sect. C: Struct. Chem.* **2015,** *71* (1), 3-8.

16. Palmer, D. C. *Crystalmaker*, CrystalMaker Software Ltd: Begbroke, Oxfordshire, England.

17. Zhao, J. K.; Gao, C. Y.; Liu, D., The extended Q-range small-angle neutron scattering diffractometer at the SNS. *Journal of Applied Crystallography* **2010,** *43* (5 Part 1), 1068-1077.

18. Arnold, O.; Bilheux, J. C.; Borreguero, J. M.; Buts, A.; Campbell, S. I.; Chapon, L.; Doucet, M.; Draper, N.; Ferraz Leal, R.; Gigg, M. A.; Lynch, V. E.; Markvardsen, A.; Mikkelson, D. J.; Mikkelson, R. L.; Miller, R.; Palmen, K.; Parker, P.; Passos, G.; Perring, T. G.; Peterson, P. F.; Ren, S.; Reuter, M. A.; Savici, A. T.; Taylor, J. W.; Taylor, R. J.; Tolchenov, R.; Zhou, W.; Zikovsky, J., Mantid—Data analysis and visualization package for neutron scattering and μ SR experiments. *Nuclear Instruments and Methods in Physics Research Section A: Accelerators, Spectrometers, Detectors and Associated Equipment* **2014,** *764*, 156-166.

19. Wignall, G. D.; Bates, F. S., Absolute calibration of small-angle neutron scattering data. *Journal of Applied Crystallography* **1987,** *20* (1), 28-40.

20. Motokawa, R.; Suzuki, S.; Ogawa, H.; Antonio, M. R.; Yaita, T., Microscopic Structures of Tri-n-butyl Phosphate/n-Octane Mixtures by X-ray and Neutron Scattering in a Wide q Range. *The Journal of Physical Chemistry B* **2012,** *116* (4), 1319-1327.

21. Frisch, M. J.; Trucks, G. W.; Schlegel, H. B.; Scuseria, G. E.; Robb, M. A.; Cheeseman, J. R.; Scalmani, G.; Barone, V.; Mennucci, B.; Petersson, G. A.; Nakatsuji, H.; Caricato, M.; Li, X.; Hratchian, H. P.; Izmaylov, A. F.; Bloino, J.; Zheng, G.; Sonnenberg, J. L.; Hada, M.; Ehara, M.; Toyota, K.; Fukuda, R.; Hasegawa, J.; Ishida, M.; Nakajima, T.; Honda, Y.; Kitao, O.; Nakai, H.; Vreven, T.; Montgomery Jr., J. A.; Peralta, J. E.; Ogliaro, F.; Bearpark, M. J.; Heyd, J.; Brothers, E. N.; Kudin, K. N.; Staroverov, V. N.; Kobayashi, R.; Normand, J.; Raghavachari, K.; Rendell, A. P.; Burant, J. C.; Iyengar, S. S.; Tomasi, J.; Cossi, M.; Rega, N.; Millam, N. J.; Klene, M.; Knox, J. E.; Cross, J. B.; Bakken, V.; Adamo, C.; Jaramillo, J.; Gomperts, R.; Stratmann, R. E.; Yazyev, O.; Austin, A. J.; Cammi, R.; Pomelli, C.; Ochterski, J. W.; Martin, R. L.; Morokuma, K.; Zakrzewski, V. G.; Voth, G. A.; Salvador, P.; Dannenberg, J. J.; Dapprich, S.; Daniels, A. D.; Farkas, Ö.; Foresman, J. B.; Ortiz, J. V.; Cioslowski, J.; Fox, D. J. *Gaussian 09*, Gaussian, Inc.: Wallingford, CT, USA, 2009.
22. Zhao, Y.; Truhlar, D. G., The M06 suite of density functionals for main group thermochemistry, thermochemical kinetics, noncovalent interactions, excited states, and transition elements: two new functionals and systematic testing of four M06-class functionals and 12 other functionals. *Theoretical Chemistry Accounts* **2007,** *120* (1), 215-241.
23. (a) Boys, S. F.; Bernardi, F., The calculation of small molecular interactions by the differences of separate total energies. Some procedures with reduced errors. *Molecular Physics* **1970,** *19* (4), 553-566; (b) Simon, S.; Duran, M.; Dannenberg, J. J., How does basis set superposition error change the potential surfaces for hydrogen‐bonded dimers? *The Journal of Chemical Physics* **1996,** *105* (24), 11024-11031.
24. Aleksenko, S. S.; Gumenyuk, A. P.; Mushtakova, S. P.; Timerbaev, A. R., Speciation studies by capillary electrophoresis – distribution of rhodium(III) complexed forms in acidic media. *Fresenius' Journal of Analytical Chemistry* **2001,** *370* (7), 865-871.
25. Geswindt, T. E. Chemical speciation of RhIII complexes in acidic, halide-rich media by means of 103Rh NMR spectroscopy : the importance of speciation in the selective separation and recovery of rhodium. Stellenbosch University, 2013.
26. Gerber, W. J.; Koch, K. R.; Rohwer, H. E.; Hosten, E. C.; Geswindt, T. E., Separation and quantification of [RhCln(H2O)6−n]3−n (n = 0–6) complexes, including stereoisomers, by means of ion-pair HPLC–ICP-MS. *Talanta* **2010,** *82* (1), 348-358.
27. Cotton, F. A.; Ucko, D. A., The structure of trimethylphenylammonium nonachlorodirhodate(III) and a survey of metal-metal interactions in confacial bioctahedra. *Inorganica Chimica Acta* **1972,** *6*, 161-172.
28. (a) Levitin, G.; Schmuckler, G., Solvent extraction of rhodium chloride from aqueous solutions and its separation from palladium and platinum. *Reactive and Functional Polymers* **2003,** *54* (1–3), 149-154; (b) Afzaletdinova, N. G.; Khisamutdinov, R. A.; Bondareva, S. O.; Murinov, Y. I., Rhodium(III) extraction from aged hydrochloric acid solutions with triacylated pentaethylenehexamine trihydrochloride. *Russ. J. Inorg. Chem.* **2015,** *60* (12), 1583-1587.
29. Bilbeisi, R. A.; Prakasam, T.; Lusi, M.; El Khoury, R.; Platas-Iglesias, C.; Charbonnière, L.

J.; Olsen, J.-C.; Elhabiri, M.; Trabolsi, A., [C–H···anion] interactions mediate the templation and anion binding properties of topologically non-trivial metal–organic structures in aqueous solutions. *Chemical Science* **2016,** *7* (4), 2524-2531.

30. MacRuary, K. J.; Gordon, R. J.; Grant, R. A.; Woollam, S.; Ellis, R. J.; Tasker, P. A.; Love, J. B.; Morrison, C. A., On the Extraction of HCl and H2PtCl6 by Tributyl Phosphate: A Mode of Action Study. *Solvent Extraction and Ion Exchange* **2017,** *35* (7), 531-548.

31. (a) Moyer, B. A.; Bonnesen, P. V.; Custelcean, R.; Delmau, L. H.; Hay, B. P., Strategies for using host-guest chemistry in the extractive separations of ionic guests. *Kem. Ind.* **2005,** *54* (2), 65-87; (b) Hofmeister, F., Zur Lehre von der Wirkung der Salze - Zweite Mittheilung. . *Arch. Exp. Pathol. Pharmakol.* **1888,** (24), 247-260.

Graphical Abstract

Encapsulation of $RhCl_5(H_2O)^{2-}$ by aminoamide receptors permits very efficient rhodium recovery by solvent extraction